IRAS Observations of the Rho Ophiuchi Infrared Cluster: Spectral Energy Distributions and Luminosity Function

PREPRINTS
OF THE
STEWARD OBSERVATORY
THE UNIVERSITY OF ARIZONA
TUCSON, ARIZONA 85721, U.S.A.

No. 848

IRAS OBSERVATIONS OF THE ρ OPHIUCHI INFRARED CLUSTER: SPECTRAL ENERGY DISTRIBUTIONS AND LUMINOSITY FUNCTION

Bruce A. Wilking,[1]

Department of Physics
University of Missouri - St. Louis

and

Charles J. Lada,[1] and Erick T. Young[1]

Steward Observatory, University of Arizona

To appear in Astrophysical Journal, May 15, 1989

1 Visiting Astronomyer at the Infrared Telescope Facility, which is operated by the University of Hawaii under contract from the National Aeronautics and Space Administration.

ABSTRACT

We present an analysis of high sensitivity IRAS coadded survey data and Pointed Observations toward a 4.3 pc^2 area comprising the central star-forming cloud of the Ophiuchus molecular complex. Using near-infrared and Hα surveys, we are able to associate 44 of the 64 IRAS 12μm point sources in this region with young stellar objects. As a result, a total of 78 YSOs are now established as members of this dust-embedded cluster. By synthesizing the visible/near-infrared data with that from IRAS, we have constructed spectral energy distributions and estimated bolometric luminosities for the majority of embedded sources. We have classified each spectral energy distribution into the classification scheme of Lada and Wilking by using the spectral index in the 2.2-25 μm wavelength interval. The shapes of the spectral energy distributions form a continuous sequence from heavily obscured objects (Class I) to T Tauri stars (Class II); with the aid of the theoretical models of Adams, Lada, and Shu, we interpret this as an evolutionary sequence from accreting protostars (Class I) to pre-main-sequence objects with circumstellar disks (Class II). From the relative number of objects in each evolutionary state, we are able to estimate crudely the lifetime of the accretion phase, the mass accretion rate, and the duration of star formation in Ophiuchus. Our analysis suggests that the relatively high star formation efficiency in the core of the cloud (SFE > 22%) is the result of an efficient burst of star-forming activity which has occurred over the last few million years. The luminosity function of the embedded cluster is also constructed. A remarkable feature of the luminosity function is the segregation of source luminosities by the shapes of their spectral energy distributions. The dominance of Class I objects at intermediate luminosities suggests that either stars undergo luminosity evolution as they progress from Class I to Class II objects or that stars in the cloud are being formed sequentially in mass. The observed luminosity function represents a direct measurement of the true

original luminosity function of the embedded cluster. The relationship between the observed luminosity function and that derived from the Initial Mass Function is discussed.

Subject headings: clusters: open - infrared: sources - luminosity function - spectrophotometry - stars: pre-main-sequence - nebulae: individual

I. INTRODUCTION

In our galaxy, the formation and evolution of stars takes place within dense molecular clouds. Consequently, it is reasonable to expect young stellar objects (YSOs) to be physically associated with varying amounts of interstellar gas and dust which will affect their observed appearance. Indeed, the youngest objects (e.g., protostars) should be rendered completely invisible by the obscuration of opaque (at visual wavelengths) circumstellar dust. In such circumstances a significant fraction of the luminous energy of a YSO will be radiated in the infrared. Since the circumstellar material associated with YSOs is distributed throughout a volume of space considerably larger than that of the young star itself, the resulting emission will be likely radiated over a wavelength range larger than that expected from a single temperature blackbody or photosphere (e.g., Lada 1987). Therefore, to investigate the nature of the youngest stellar sources requires observations over a wide range of infrared wavelengths (i.e., 1 to 100 μm). Such observations have shown that the infrared energy distributions of YSOs exhibit well-defined structure (i.e., Lada and Wilking 1984; Myers et al. 1987). The source to source variation in the shapes of their energy distributions can be used to classify YSOs into broad but distinct morphological groups, which appear to represent phases in an evolutionary sequence from protostar to main sequence star (i.e., Lada 1987; Adams, Lada and Shu 1987). In addition, integration over the infrared energy distributions provides relatively accurate determinations of the bolometric luminosities of young stellar objects (Lada and Wilking 1984, hereafter LW). Study of source energy distributions, therefore, may be a powerful probe for investigating star formation and early stellar evolution.

It would be extremely useful to make a comparative study of source energy distributions for the entire embedded population of YSOs in an individual star-forming cloud. A systematic investigation of a reasonably complete sample of newly formed objects from the same formation site would be potentially capable of addressing some fundamental issues concerning star formation including: the overall duration of star formation activity in a cloud, the relative duration of the various phases of early stellar evolution, the luminosity evolution of young stellar objects, the role of energetic outflow activity in early stellar evolution, the nature of the initial luminosity function and the origin of the initial mass function.

The nearby ρ Ophiuchi molecular cloud is a prime site for the type of systematic investigation described above. Its centrally condensed core harbors an unusually high density of young stellar objects (Grasdalen, Strom and Strom 1973; Vrba et al. 1975; Elias 1978; Wilking and Lada 1983) which are primarily of low luminosity and presumably low mass (Fazio et al. 1976; Wilking and Lada 1983; LW; Cudlip et al. 1985; Young, Lada and Wilking 1986). Because of the relatively high star formation efficiency and the quiescent conditions in the cloud core, it has been suggested that a gravitationally bound cluster similar to the Pleaides will ultimately emerge from the cloud (Wilking and Lada 1983; Lada, Margulis and Dearborne 1984). An initial study of the nature of the embedded population in the Ophiuchus cloud was made by

LW. They constructed energy distributions from 1-20 μm for more than 30 sources in the cloud and showed that the sources could be grouped into three distinct spectral classes depending on the shapes of their energy distributions. They also determined a luminosity function for the embedded sources which appeared to be deficient in intermediate luminosity stars compared to that of the initial luminosity function for field stars. However, these observations and their analysis were limited by the lack of data at far-infrared wavelengths where a significant portion of the YSO luminosities are radiated. Furthermore, since the sources studied were selected from inhomogenous and incomplete near-infrared surveys of the cloud, it was not clear how representative they were of the entire embedded population.

In principle, these limitations can be overcome by analysis of the far-infrared observations of this region obtained by IRAS. The IRAS observations completely sample the entire extent of the cloud with relatively high sensitivity, providing a complete census of far-infrared emission from the region. With these observations it is possible to obtain a more complete and representative sample of the embedded population of the cloud as well as more complete energy distributions and more accurate bolometric luminosities for the embedded sources. An analysis of the IRAS high resolution Pointed Observations of a 1.5 pc^2 region which comprises most of the high extinction core of the cloud has been presented by Young, Lada and Wilking (1986; hereafter Paper I). In this paper, we use IRAS coadded survey data, coupled with new high sensitivity near-infrared observations, to investigate the nature of embedded objects over a much larger area (4.3 pc^2) of the cloud. This larger area, shown in Figs. 1a and 1b, encompasses the central cloud of the ρ Ophiuchi complex and includes the core region. The boundaries for the region of study correspond to the contour of ^{13}CO emission where T_R^* (^{13}CO, 1-0) = 6 K (Loren 1988) and A_V ~ 4.5 mag (assuming an excitation temperature of 25 K, Dickman 1978).

Combining the IRAS and near-infrared data sets enables us to identify a total of 78 members of the embedded cluster. Spectral energy distributions are constructed for 53 objects and are compared with theoretical models to gain insight into their evolutionary status. Bolometric luminosities can be estimated for nearly all of the association members leading to a revised luminosity function for this dust-embedded cluster.

II. Observational Procedure and Equipment

A. IRAS Data Analysis

The first step in the analysis of the IRAS data was the identification of point or small extended sources in the 12 μm and 25 μm data bases. For this purpose, we examined three high sensitivity data sets: high resolution Pointed Observations of the core (Paper I), survey resolution Pointed Observations MC2169 (centered on $16^h23^m44\overset{s}{.}0$, $-23^\circ 59'22''$) and MC0016 (centered on $16^h24^m15\overset{s}{.}6$, $-24^\circ35'42''$), and coadded survey data. The full-width at half power (FWHP) resolution of these later two data sets in the 12 and 25 μm bands was 45" in the in-scan direction (roughly north-south in declination) and 210" in the cross-scan direction.

Positions and flux densities of sources not already presented in Paper I were determined exclusively from in-scan slices through each source using coadded survey data. As an example, in-scan slices of IRAS 34 at 12 and 25 μm are shown in Fig. 2 and are typical of many sources in the cloud. The baseline chosen to subtract out the extended plateau of emission (usually present in all bands) is indicated. From this slice, one can isolate the emission of IRAS 34 from surrounding sources. After baseline subtraction, the source flux density was determined by comparing the width of the emission profile with that expected by a point source (45").

Photometric calibration was based upon the same absolute calibration as the IRAS Point Source Catalog (1985). We estimate the photometric uncertainties to be ±15% in regions of low source density and increasing to as high as ±50% in confused regions. These larger uncertainties are most prevalent in the 60 μm and 100 μm bands where the source confusion is most serious. No color corrections were made to the source flux densities; these corrections are less than 10% since the 12-100 μm energy distributions are generally flat or decreasing in λF_λ.

The completeness limit of the IRAS coadded survey data is difficult to estimate due to the variable source density across the field. In regions of low source density, the reliable (4.5-5σ) detection limit at 12 μm is roughly 3 times more sensitive than the main survey, i.e, $F_\nu(12\ \mu m) = 0.15$ Jy. Sources with flux densities at this level are unreliable in confused regions. A reliable detection limit in heavily confused areas at 12 μm is about 1.0 Jy.

In addition to the 18 IRAS sources identified in high resolution observations of the cloud core (Paper I), 46 point or small extended sources were extracted from adjacent regions. The positions and fluxes estimated for these sources are given in Table 1 along with the FWHP of the source in the in-scan direction. The positions are reliable to within roughly 15" in declination and 30" in right ascension for strong, unconfused sources. Since we bin the flux from all detectors for a given source, this positional accuracy is slightly poorer than that of the Point Source Catalog. The positions of these 64 IRAS sources are shown in Fig. 1a superposed on the red POSS photograph and relative to the approximate boundary of the molecular cloud. Large crosses denote sources with 12 μm flux densities greater than 0.25 Jy and small crosses less than this value. For comparison, the IRAS 12 μm coadded intensity map of the same region is presented in Fig. 1b, indicating the prevalence of low-level extended emission across most of the entire cloud.

Only 24 of these 64 sources are listed in the Point Source Catalog. The higher sensitivity of the Pointed Observations and coadded survey is primarily responsible for our larger sample. The high resolution Pointed Observations have enabled us to resolve 3 multiple sources confused in the Point Source Catalog.

B. The Identification of Candidate Optical/Near-Infrared Counterparts

High resolution near-infrared (typically 6-12" beam size) and Hα objective prism surveys can be used to identify YSOs which are associated with the IRAS emission. Two-micron sources and Hα stars which lie within 20" and 45" of the IRAS 12 μm position in the in-scan and cross-scan directions were considered as candidates. Near-infrared sources with slightly larger offsets in the in-scan direction were admitted as counterparts for IRAS sources extended by more than 45" (e.g., IRAS 9). For three of the weaker 12 μm point sources, 2 μm objects were located within 70-90" of the more uncertain cross-scan position (but within 4" in declination) and had near-infrared energy distributions which joined smoothly with the IRAS data. We have assumed these objects are associated with IRAS emission but confirmation of this association is needed (see col. 10 of Table 1). Published surveys of the ρ Oph cloud were used when possible to identify possible optical/near-infrared counterparts (Vrba et al. 1975; Elias 1978; Wilking and Lada 1983; Wilking, Schwartz and Blackwell 1987). However, since only select regions of the cloud have been surveyed with sensitive 2 μm observations, we were obliged to obtain an extensive new set of near-infrared observations which are described in the next section.

C. IRTF Observing Procedure

All ground-based infrared observations reported here were obtained using the 3 meter telescope and facility instruments of the Infrared Telescope

Facility (IRTF) located at Mauna Kea, Hawaii. The data were collected in 1984 July, 1985 April, and 1986 June. A small subset of these data have been previously presented in Paper I. The identification of the IRAS near-infrared counterparts involved several types of observations. First, 2 μm maps of a one square arcmin region centered on the IRAS 12 μm position were obtained using a 7.5" beam with a 60" chopper throw and with beam-switching disabled. The (3σ) detectable limit of the maps was always better than 14 mag at K. Because of the larger FWHP of the IRAS beam in the cross-scan direction, it was sometimes necessary to map adjacent fields in right ascension to locate a candidate source. Forty-two fields were mapped toward 26 IRAS sources, revealing at least one 2 μm object for 23 IRAS sources. The IRAS sources mapped in this study and the 2 μm sources revealed are indicated in columns 9 and 10 of Table 1. The positions of the 2 μm sources detected in these surveys (with IRS designations) are presented in Table 2, determined by offsets from nearby SAO stars through the broadband K filter. They are accurate to within 1.5".

The second step in the observations was to obtain near-infrared broadband photometry for the candidate 2 μm counterparts. Sources with steeply rising energy distributions and infrared excesses were selected for mid-infrared photometric observations. Photometry presented in Table 2 was obtained using both the InSb (1.25-3.4 μm) and bolometer systems (4.8-20 μm) through either a 3mm (5.5") or 4mm (7.5") aperture. Photometric infrared magnitudes were determined relative to infrared standard stars including a secondary J through L standard, HD147889, established within the cloud. Unless otherwise indicated in Table 2, statistical one sigma errors in the photometry were less than 0.03 mag at J through K, 0.05 at L, 0.1 at M and N, and 0.2 at Q.

III. Results

A. The Success of Identifying Optical/Near-Infrared Counterparts to IRAS Sources

We assumed initially that the positional coincidence of a 2 μm source or Hα star with an IRAS source was sufficient evidence to associate it with the IRAS emission. This association was usually borne out by 10-20 μm photometry and/or a match between the near-infrared and far-infrared energy distribution. However, for three IRAS sources (20, 21, and 35) there is not a good match between the IRAS data and the colors of the corresponding near-infrared sources. These associations are regarded as uncertain and these sources have not been included in subsequent discussions of the spectral energy distributions and luminosity function. About twenty-five percent of the IRAS sources with possible Hα or near-infrared counterparts had multiple candidates. In most of these cases, a single counterpart could be identified which dominated at 10 μm and/or had a near-infrared energy distribution which joined most smoothly with the IRAS data. For only three IRAS sources (3,11, and 17), the relative contribution of two near-infrared sources to the IRAS emission could not be disentangled. One would expect that a close agreement between the ground-based 10 μm flux of a near-infrared source with the IRAS 12 μm flux would best establish it as the near-infrared counterpart. However, as discussed in the following section, this criterion fails due to the prevalence of extended mid-infrared emission.

Among the 64 IRAS sources considered, 44 were successfully identified with their YSO counterparts, a success rate of ~70%. Of these 44, 28 associations were made using published 2 μm or Hα surveys. Our new near-infrared observations led to the confirmation of 7 of these associations plus the identification of 16 additional IRAS sources with their near-infrared counterparts. Of the remaining 20 sources, seventeen were not surveyed at 2 μm and had no previously known optical/near-infrared counterpart.

Our failure to associate 20 of the IRAS sources with their YSO counterparts leaves us uncertain as to their nature. The dust emission toward these sources (e.g., IRAS 22) could arise from a clump externally heated by neighboring early B stars, particularly the B2V star HD 147889 (Garrison 1967, Young and Greene 1988). Source counts at 12 μm for the galactic latitude of ρ Oph and extrapolated to the sensitivity of the coadded survey data suggest that as many as 10 sources in our sample could be background objects. Likewise, the absence of a 2 μm source could imply the YSO is too heavily obscured to be detected by near-infrared observations. Sensitive images of these IRAS sources with the new generation of near-infrared cameras are needed to determine their true nature. The exclusion of these 20 sources, should they have intrinsic sources of luminosity, should not seriously affect our study of the cluster luminosity function since most are members of a low-luminosity population incompletely-sampled by IRAS. Only six have 12 μm flux densities greater than 1 Jy and only one of these was detected in more than two of the IRAS bands.

A check was performed to insure that 2 μm sources found associated with IRAS emission were indeed YSOs embedded in the cloud. As detailed in Appendix A, we have applied a set of criteria to each 2 μm source known to lie toward this region of the ρ Oph cloud in an effort to distinguish between YSOs and background field stars. The results of this classification scheme are presented in Tables 1-3 in Appendix A and in column 14 of Table 2. One IRAS source in our study was found to be associated with a background field star (IRAS 27/EL15). The vast majority of 2 μm sources associated with IRAS emission through positional coincidence were classified as YSOs in our scheme, primarily through the presence of an infrared excess in the 2.2-25 μm spectral region.

B. The Nature of Extended IRAS 12 μm Emission

In the course of our study, we have encountered extended emission in the

IRAS 12 μm data on three different size scales. In all cases, the extended emission cannot be explained by equilibrium heating of normal interstellar grains. First, low-level 12 μm emission extended on a scale of tens of arcminutes is evident in the intensity map of the cloud (Fig. 1b). This component most likely arises from nonequilibrium heating of very small dust grains at the surface of the cloud by the B2V star HD147889 (Paper I, Young and Greene 1988).

Second, in-scan slices have revealed that the FWHP of the 12 μm emission for eleven of the sources is extended relative to the 45" IRAS beam (e.g., see Fig. 2). As shown in column 8 of Table 1, source profiles have FWHP's ranging from 60-210 arcsec. This extended component could be due to multiple 12 μm sources unresolved by the IRAS beam. Five of the 12 sources have not been surveyed with high sensitivity 2 μm surveys and multiplicity cannot be ruled out. However for six sources, sensitive 2 μm surveys have revealed only single sources and the presence of multiple candidates appears unlikely. It is plausible that for two of these objects, IRAS 36 (Source 1) and IRAS 28 (SR3), their associated stars (B3-B5V and B9-A0V, LW) have created a dust-evacuated cavity and ultraviolet photons from these stars heat very small dust grains along the cavity walls. The presence of such cavities are consistent with the morphology of the spectral energy distributions of these objects (Sec. C4). For lower luminosity YSOs without known multiple candidates such as IRAS 6 (WL1) and IRAS 9 (WL9) (see Paper I), a similar explanation for the extended emission is more problematical. Deeper 2 μm surveys will be the first step in understanding the nature of the extended emission in these sources.

Finally, as noted in Paper I, there is indirect evidence for 12 μm emission toward YSOs which is extended on scales of 6-45 arcseconds. This is indicated by the fact that the ground-based 10 μm flux of a YSO (extrapolated to 12 μm) usually falls short of the IRAS 12 μm flux by a factor of 2-3. This

is demonstrated in column 11 of Table 1. As in the case of resolved IRAS 12 μm profiles, explanations involving multiple sources or non-equilibrium heating of small dust grains are possible.

C. Spectral Energy Distributions

By synthesizing visible and near-infrared photometry of a YSO with its corresponding IRAS data, we can examine its spectral energy distribution (SED) covering a possible wavelength range from .36 μm to 100 μm. However, due to extinction at short wavelengths and confusion at 60 and 100 μm, a typical SED covers the 1.25-25 μm spectral region. The λF_λ SEDs for 32 association members with IRAS emission are presented in Figure 3 (a-e). The SED for the field star EL15 is shown in Fig. A2 of Appendix A. A λF_λ plot was adopted to utilize the fact that a flat SED indicates equal luminosity radiated by the source in each logarithmic wavelength interval (e.g., Disney and Sparks 1982; Lada 1988).

Sources in Fig. 3 are grouped according to the morphology of their SEDs which is described quantitatively by the spectral index "a" in the 2.2-25 μm spectral region (Lada 1987, see Appendix A). In addition to the sources in Fig. 3 and A2, we have derived spectral indices for association members and field or unidentified stars which had existing 10 μm or 20 μm photometry but no measured IRAS emission due to confusion. Spectral indices for a total of 53 objects are presented in Table 3. The SEDs for many of these latter objects have been presented by LW.

For our discussion of the SEDs, we will adopt the classification scheme devised by Lada (1987): Class I objects have $a>0$ (Fig. 3a and 3b), Class II objects have $-2<a<0$ (Fig. 3c and 3d), and Class III sources have $a<-2$. As one can see by comparing these SEDs with those of blackbodies in Fig. 3c and 3e, the energy distributions for Class I and II objects are much broader than a single temperature blackbody. Class III SEDs resemble those of reddened blackbodies. SEDs which exhibit two distinct peaks are plotted separately in Fig. 3e. While these double-peaked distributions cannot be characterized by a single spectral index, we have expanded Lada's classification scheme to accommodate them (Section C4). We now consider each of these morphological groups separately.

1) Class I Objects - Sources with positive spectral indices are the coldest and most deeply embedded YSOs displaying little or perhaps no emission from a stellar photosphere. The emergent flux arises primarily from dust at a wide range of temperatures. These SEDs are unique because of the large quantities of hot dust (T~300-1000 K) close to the star which radiate between 3.4 and 12 μm. Consistent with the deeply embedded state of Class I objects is the fact that only two of the 24 Class I objects in our sample (IRS48 and DoAr 25) are visible on the red POSS photograph (m < 20.0 mag).

2) Class II Objects - The energy distributions for objects with spectral indices less than zero but greater than -2 are dominated by a stellar photosphere reddened by foreground extinction. There is usually some excess emission due to hot dust in the 3.4-12 μm spectral region but, as shown in Fig. 3c and 3d, no evidence for a substantial cooler dust (~50-100 K) component as is present in Class I objects. The 27 Class II objects include five of the six T Tauri stars which are observed to have mid-infrared emission. (The sixth, SR4, has a cool dust component and is classified as Class IID). The average value of "a" for the Class II stars in our sample is -0.65 with a sample standard deviation of 0.34. Rucinski (1985) has analysed energy distributions for 35 T Tauri stars in the Taurus-Auriga complex with 12-100 μm IRAS emission. Most have Class II SED's with a=-1 or shallower. This suggests that most of the Class II objects in our sample are in a T Tauri phase of evolution.

3) Class III Objects -Only one source in our sample has a spectral index <-2. VSSG16 has been classified as a field star (Elias 1978, Appendix A) and has a SED resembling those in Fig. A2. The scarcity of Class III objects in our sample is perhaps surprising. However, it is probable that we have selected against their detection by considering sources identified with far-infrared emission. Further photometric observations may reveal Class III objects among the forty-nine 2 μm sources which include YSOs not associated with IRAS emission and "unidentified" sources (see Appendix A).

4) Double-Peaked Energy Distributions - Four energy distributions are presented in Fig. 3e which have two distinct peaks, hence a single spectral index does not define the spectral shape. One peak occurs near 1.6 μm and arises from a reddened photosphere. The second peak occurs in the far-infrared and is due to cooler dust. All four objects are visible stars. The star GSS23 has a similar SED. Several of the objects we have classified as Class I or II may fall into this category but due to the lack of UBVRI photometry, 4.8 μm photometry, or the presence of confusion at 60 and 100 μm, both peaks are not well defined.

Two of the sources in Fig. 3e, Source 1 and SR3, are among the most luminous sources in the infrared cluster and have been classified as B3-B5V and B9-A0V, respectively (LW). Their energy distributions are reminiscent of stars associated with reflection nebulosity (e.g., Harvey, Wilking, and Joy 1984). These objects have dissipated their inner circumstellar dust and now excite emission from cool dust much further removed from the star. We classify these objects as Class IIID; because of the lack of hot dust, the first peak in their SED resembles that of a Class III object. The B2V star HD147889 which excites extensive optical reflection nebulosity in the western regions of the cloud and the x-ray star GSS23 are also classified as Class IIID objects (Young and Greene 1988, LW).

The remaining double-peaked SEDs are found for two lower-luminosity objects: SR4, a T Tauri star, and SR21. Their SEDs do not show the sharp drop in λF_λ from 1.6-4.8 μm present for Source 1 and SR3. The larger amounts of hot circumstellar dust present in these objects lead us to associate them with Class II rather than Class III objects. Hence the SEDs for SR4 and SR21 are classified as Class IID.

D. Luminosity Estimates for Association Members

1. The Calorimetric Technique

We define the "observed luminosity" to be the total energy per second radiated by a YSO:

$$L(\mathrm{obs}) = 4\pi d^2 \int_0^\infty F_\lambda d\lambda = (9.2)\pi d^2 \int_0^\infty \lambda F_\lambda \; d(\log_{10}\lambda) \qquad (1)$$

where F_λ is the flux density per unit wavelength and d is the distance to the YSO. Equation 1 assumes that the luminosity is radiated isotropically by the source. By integrating the SED of an object over the observed range of wavelengths, we obtain an estimate for the observed luminosity:

$$L'(\mathrm{obs}) = (9.2)\pi d^2 \int_{\lambda_i}^{\lambda_f} \lambda F_\lambda d(\log_{10}\lambda) \qquad (2)$$

where λ_i, λ_f are the shortest and longest wavelength observed, respectively, and d is the distance to the ρ Oph complex (160 pc, Elias 1978).

The degree to which equation 2 accurately approximates L(obs) depends upon the ability of IRAS to recover most of the stellar luminosity which is absorbed by dust at shorter wavelengths and re-radiated in the far-infrared. A flattening or turnover in the λF_λ vs. log λ plot of the energy distribution at λ_f is a strong indication that the bulk of the source luminosity is radiated over the

wavelength interval observed. However, for many Class I objects (a > 1.0), the SED is often still rising at 60-100 μm (see Fig. 2a). In order to account for the luminosity radiated by cooler dust (T_d < 30 K), we derive a second estimate for L(obs) which extrapolates the SED to $\lambda_f = \infty$:

$$L''(\mathrm{obs}) = (9.2)\pi d^2 \int_{\lambda_i}^{\infty} \lambda F_\lambda d(\log_{10}\lambda) \qquad (3).$$

We assume that the flux density from λ_f to ∞ falls off with a spectral index of a = -1 which is similar to the long wavelength slope of the SED for T Tauri stars. This extrapolation is much shallower than the spectral index of the Rayleigh-Jeans portion of a corresponding blackbody curve (a = -3).

The values for L'(obs) and L"(obs) for 74 association members are presented in Table 3 along the corresponding wavelength interval (λ_i,λ_f) for each estimate. Also presented in Table 3 is L(fir), the luminosity radiated across the 4 IRAS bands.

IV. Implications

A. Spectral Energy Distributions

1) A Possible Evolutionary Sequence?

It has been suggested by Lada (1987) and Adams, Lada, and Shu (1987, hereafter ALS) that the different SED shapes represent a quasi-continuous evolutionary sequence for low mass stars (where radiation pressure is minimal, M < $7M_\odot$). This suggestion is based upon theoretical models which describe the emergent flux from YSOs (Adams and Shu 1986, ALS, Myers et al. 1987). Simply stated, these models decompose the SED of a YSO into contributions from a reddened gas photosphere (visible to near-infrared emission), a dusty disk (mid-infrared), and a spherical dust envelope (far-infrared). In the ALS scenario, Class I objects represent the earliest evolutionary state of a pre-main sequence object and are modeled as a rotating protostar comprised of a gas photosphere (the accretion shock), dusty disk, and infalling dust envelope. The emergent flux, dominated by the spherical dust envelope, is the result of infall accretion luminosity. The energy distributions for Class I objects EL29, WL16 and WL22 from this study have been fit by ALS using this model.

The accretion phase is interrupted by a strong stellar wind which reverses the infall and begins to clear away the surrounding dust envelope thus revealing the embedded star plus disk. At this point, the object begins its PMS contraction along a convective track. The resulting SEDs are double-peaked, the far-infrared emission arising from this residual envelope. The energy distribution for the Class IID object SR21 (=VSSG23, see Fig. 2e) is well fit by this model (ALS).

As the strong stellar wind completes the clearing of the dust envelope, the energy distribution will be dominated by the stellar photosphere plus dust disk, i.e, a Class II/T Tauri SED. The energy distributions of Class objects have been modeled by ALS assuming a photosphere plus dusty passive disk which absorbs approximately 25% of the stellar luminosity (e.g., the T Tauri star SR9). However, the far-infrared spectral index produced by a passive disk (and also an optically-thick accretion disk) is -1.33 and steeper than observed for most Class II objects (e.g., this study, Rucinski 1985). The shallower SED for Class II objects implies a smaller temperature gradient ($r^{-0.6}$) than proposed for the model disks ($r^{-0.75}$). Such a temperature gradient could result from a flaired passive disk (Kenyon and Hartmann 1987) or from a disk with intrinsic luminosity arising from nonviscous accretion (Adams, Lada, and Shu 1988).

Finally, as the star approaches the main sequence, the circumstellar disk will be dissipated. The resulting SED resembles that of a blackbody reddened by foreground extinction. These Class III objects represent the post T Tauri

phase of evolution and can be identified through proper motion studies (Jones and Herbig 1979), x-ray emission (Walter 1986) or weak emission lines in the optical (e.g., Herbig, Vrba and Rydgren 1986).

The distribution of the SEDs presented in Fig. 4 is consistent with the idea of an evolutionary connection between Class I and Class II objects. Namely, there is a continuous distribution of spectral indices from deeply embedded objects ($a>1.0$) to T Tauri stars ($a = -0.65$) in the ρ Oph cluster. Myers et al. (1987) present a similar plot for stars found in the vicinity of dense molecular cores defining the spectral index as $s=a+1$. Their histogram is similar to that in Fig. 4 except for a pronounced dip in their data at $a=0.4$.

2) Duration of the Embedded State

If the dispersion in spectral indices represents a true variation in the evolutionary states between the cluster members, then we can crudely estimate the lifetime of the embedded state from the relative number of Class I to Class II objects. For $L > 1L_\odot$ there are 18 Class I objects observed as compared to 15 Class II, the latter value needing to be corrected upward by 30% to account for the incomplete sampling by IRAS of 1 $L_\odot$ Class II objects. Therefore, the nearly equal numbers of Class I and II objects suggests that, given a constant birthrate, the average lifetime of stars in the embedded state is comparable to the average lifetime of the T Tauri (Class II) stars in the cloud. We have estimated the ages of eight T Tauri stars in the ρ Oph cloud in the 0.4 -1.0 $M_\odot$ range. We have used the data of Cohen and Kuhi (1979) to derive the Kelvin-Helmholtz contraction time for each star since the end of the accretion phase (e.g., Stahler 1983). The resulting ages for the T Tauri stars since their appearance at the "birthline" range from 0-1.5 x 10^6 years; the average age is 3.9 ± 1.7 x 10^5 years. If Class I objects are in the accretion phase of their evolution as suggested by the ALS models, this implies that the accretion phase lasts about 4×10^5 years and that the mass accretion rate is ~ 2.5×10^{-6} $M_\odot$/yr for a 1 $M_\odot$ star.

We view our estimate for the duration of the accretion phase as an upper limit and hence the mass accretion rate as a lower limit. First, as we will discuss in Section B3, many of the lower luminosity Class II objects (L ~ 1 $L_\odot$) may have evolved from intermediate luminosity Class I objects (L > 10 $L_\odot$). Thus if we instead compare the number of intermediate luminosity Class I objects (nine) with the number of Class II objects with L > 1 $L_\odot$ (twenty), we derive an estimate of 2×10^5 years for the Class I phase and 5×10^{-6} $M_\odot$/yr for the mass accretion rate. Second, it has been suggested that some fraction (perhaps 50%) of the Class I objects evolve rapidly through the Class II phase and become Class III objects while still in the convective phase of their PMS evolution (e.g., the naked T Tauri stars, Walter 1986, Walter et al. 1988). Thus, accounting for the possibility that there is a population of naked T Tauri stars equal in size to the observed Class II population, our estimate for the duration of the Class I phase would decrease by a factor of 2 and the mass accretion rate would double. It is interesting to note that consideration of these two effects suggests a mass accretion rate similar to the value of 10^{-5} $M_\odot$/yr derived by ALS for the ρ Oph cloud considering the collapse of an isothermal sphere with a sound speed of 0.35 km s^{-1}.

3) The Duration of Star Formation in the Central Cloud

One estimate for the age of the embedded cluster and the duration of star formation in the central cloud is obtained by determining the contraction time for the least massive star on the main sequence, i.e., the contraction age. The only stars in the cluster which appear to have reached the main sequence are HD147889, Source 1, and SR3 (LW). Analysis of the SED of SR3 by LW suggests it is a B9-A0 star and the least massive cluster member on the main

sequence. The contraction time for a 3 $M_\odot$ object to the ZAMS (final point of minimum luminosity) is 1.46×10^6 years (Iben, 1965). This is consistent with our estimate for the age of the oldest T Tauri star, SR22, of 1.5×10^6 years.

An upper limit to the duration of star formation can be determined by estimating the number of Class III objects in the central cloud. While we have identified only one Class III object in our study, there may be many other such objects in the cloud that have escaped detection because they are not strong mid and far-infrared emitters. However, we can use the 2 μm survey of a 105 sq. arcmin region of the core by Wilking and Lada (1983) to set an upper limit to the Class III population. There were four objects found in their survey which had little or no infrared excess and are candidates for Class III sources (although none are visible stars). Over the same region, the 2 μm survey revealed 3 Class II objects. Thus assuming the stellar surface densities of Class II and candidate Class III objects are constant across the entire 4.3 pc^2 of the central cloud, we can infer that there are roughly equal numbers of Class III and Class II objects in the cloud.

If we assume that all the potential Class III sources are embedded in the cloud and are PMS stars, their estimated population suggests that the duration of the Class III phase of evolution is comparable to that of the Class II phase. If Class III stars are the products of Class II evolution (i.e., post T Tauri stars), then star formation has been active in the central cloud for a period of not longer than 3.5 million years. (This assumes that the duration of the Class II phase for sources in the cloud core has not been longer than the age of the oldest Class II source, i.e., about 1.5 million years and that the Class I phase lasts about 0.5 million years.) On the other hand, it is possible that the potential Class III sources are naked T Tauri stars. As mentioned earlier, such objects are thought to have evolved rapidly from Class I to Class III objects while still in the early convective phase of their PMS evolution. Consequently, these stars could have similar ages to the typical Class II sources in the cloud (e.g., Walter et al. 1988). If this were the case in Ophiuchus then the duration of star formation would be no longer than about 2.0 million years. In any event our estimate of the duration of star formation in the ρ Oph dark cloud, 1.5-3.5 million years is relatively short compared to the expected lifetimes of molecular clouds (i.e., 10-50 million years).

Apparently, the high star formation efficiency (> 22%; see Appendix B) in the core of the ρ Ophiuchi dark cloud must have been produced in an efficient burst of star formation activity characterized by a relatively high rate of star formation. Typically the star formation efficiency observed in a molecular cloud is low, on the order of a few percent (e.g., Cohen and Kuhi 1979; Duerr, Imhoff and Lada 1982; Lada 1987). If it were any larger, the global rate of star formation in the galaxy would be much higher than currently observed. Since the oldest PMS stars observable in such clouds have ages of order 10^7 years (e.g., Cohen and Kuhi 1979; Walter et al. 1988), the overall local rate of star formation in these clouds must be lower than that in the Ophiuchus cloud core. In other words, in order for an isolated molecular cloud to achieve a star formation efficiency of 20% or more at the typical rate of star formation, the duration of star formation in the cloud would have to be considerably in excess of 10^7 years. This is certainly not the case for the ρ Oph cloud core. These considerations suggest that at some fundamental level the star formation process in the Ophiuchus cloud core is different from that which generally characterizes molecular clouds such as the Taurus dark clouds. The origin of this difference is most likely related to

the structure of the molecular gas core of the ρ Oph dark cloud which is unusually centrally condensed (Wilking and Lada 1983). Magnetic fields may have played a pivotal role in the development of such a cloud core and the resulting high yield of young stellar objects (Shu, Adams and Lizano 1987).

B. Luminosity Function of the Embedded Cluster

1. Calculation of Bolometric Luminosities

In order to construct a meaningful luminosity function for the embedded cluster we must relate L"(obs) (as defined by equation 3) to the bolometric luminosity, L(bol), of an embedded source. The observed luminosity L(obs) is equal to L(bol) to a very good approximation provided that: a) the source's luminosity is radiated isotropically and either b) there is no extinction toward the source or c) all the extinction toward the source is produced by circumstellar dust which completely surrounds the source and reradiates the absorbed light in the near to far-infrared spectral region. LW derived a luminosity function for this cluster by assuming the conditions a and c were met for all sources. The steeply rising nature of most Class I sources indicates that they are surrounded by large quantities of circumstellar dust and the best models of these objects (Adams and Shu 1986; ALS; and Myers et al. 1987) suggest that conditions a and c are indeed satisfied. However, if a significant portion of the observed luminosity of Class II sources originates in disks, as suggested by many studies (e.g., ALS; Beall 1987; Rucinski 1985; Kenyon and Hartmann 1987), then it is unlikely that these objects would meet any of the above conditions (a-c). In this case, a bolometric correction would have to be determined and be applied to L"(obs) to obtain their true bolometric luminosities. However, we will now argue that such corrections are expected to be relatively small and that L"(obs) represents a relatively good estimate of L(bol) even for Class II sources.

The bolometric correction for a Class II source must consist of two parts. First, a correction to L"(obs) must be made to account for extinction and second, for the fact that the source's luminosity is not radiated isotropically. Normally one would be able to de-redden a YSO spectrum by using its observed H-K color index since the intrinsic H-K index is very nearly equal to zero for the temperature range characteristic of most stellar photospheres (e.g., Wilking and Lada 1983). This technique can produce accurate bolometric corrections for Class III sources (e.g., LW), however, stars with circumstellar disks (Class II sources) are expected to have intrinsic H-K indices which are appreciable and estimates of extinction from their infrared colors are not reliable. The effects of extinction can be approximately accounted for, however, if we assume that all Class II sources have energy distributions that are similar in shape and that extinction does not significantly affect their observed fluxes longward of 2 μm. We take the composite spectrum of 7 well studied T Tauri stars constructed by Adams, Lada and Shu (1988) as typical of a Class II energy distribution. By integrating this composite energy distribution first over all wavelengths and then between 2 μm and infinity, we find that $L_0^\infty(\mathrm{obs}) = 2.2\, L_{2\mu m}^\infty(\mathrm{obs})$. Since the luminosities listed in Table 3 have been determined over a wavelength range that includes data at wavelengths shorter than 2 μm, these estimates are likely to approximate the actual source luminosities to better than a factor of 2, even in the absence of an explicit correction for extinction.

The component of the emergent intensity from a Class II source which orginates in the disk is not radiated isotropically and for a given source one must know its inclination to the line-of-sight to correct for this effect. For a star plus disk system the total luminosity is given by:

$$L(\mathrm{obs}) = (1 - f_\star)L_\star + 2L_{disk}\cos(i) \qquad (4)$$

where $f_\star$ is the fraction of the stellar hemisphere occulted by the disk and $L_\star$ and L_{disk} are the intrinsic luminosities of the star and the disk, respectively (e.g., Kenyon and Hartmann 1987; Adams, Lada and Shu 1988; and Emerson 1988). For an infinitely extended, spatially thin and optically thick disk, $f_\star = \frac{1}{\pi}$ for $i \leq \frac{\pi}{2}$. As previously discussed, the Class II sources in the Ophiuchus cloud core have an average spectral index of -0.65 which is typical of T Tauri stars in general and their SEDS can be successfully (but not uniquely) modeled by a system which consists of a central star and a purely passive disk (ALS, Kenyon and Hartmann 1987; Strom <u>et al</u>. 1988). In such a circumstance, the luminosity radiated by the disk is directly related to the stellar luminosity and lies in the range 0.25 to 0.40 $L_\star$ depending upon whether the disk is spatially thin ($a = -1.33$) or slightly flared ($a \sim -0.6$). For most viewing angles, L(obs) will exceed $L_\star$, the actual bolometric luminosity of the system. For a face-on disk ($i = 0$), L(obs) = 1.5-1.8 $L_\star$ and in the worst case overestimates the intrinsic luminosity by a factor of two. Typically, therefore, the correction for source inclination and its anisotropic radiation pattern is of similar magnitude but in the opposite direction as the correction for extinction and the two effects tend to cancel. Consequently, we can assume that L"(obs) ~ L(bol) and approximates the intrinsic luminosities of both Class I and II sources to a factor of 2 or better.

2) The Empirical Luminosity Function

The distribution of observed luminosities is shown in Figure 5 for the 58 members of the embedded cluster for which good luminosities could be obtained from integration of their energy distributions. Also included are 16 sources known to be associated with the cloud but which have only upper limits to their 12 and 25 μm emission and consequently to their calculated luminosities.

The luminosity function presented in Figure 5 can be directly compared with that computed by LW for 37 embedded objects in the ρ Oph cloud. Their estimates for the bolometric luminosity were also based upon the calorimetric technique but relied largely upon ground-based data. While the area of the dark cloud considered by this study is 3 times larger than that considered by LW, only four of the 74 sources in Fig. 5 (including 2 with upper limits) lie outside the area considered by LW. The major differences between the two luminosity functions are the larger number of sources with well determined luminosities (58 vs. 37) and the greater number of intermediate luminosity objects present in the luminosity function resulting from this study. Both are a direct result of the inclusion of IRAS data; most of the new sources are colder, Class I objects of intermediate luminosity. Additionally, the luminosity estimates for objects considered by LW have been substantially improved, often increasing 50-100% as a result of the IRAS data.

3. Luminosity Segregation by SED Class

In Fig. 5 we have broken down the luminosity function by spectral index, indicating which sources are Class I, Class II or Class III. There is a marked tendency for Class I objects to dominate the population of the intermediate luminosity (i.e., $L > 5.6\ L_\odot$) bins. For example, of the thirty sources with luminosities in the range $0.5\ L_\odot < L''(\mathrm{obs}) < 5.6\ L_\odot$, ten (or 33%) are Class I objects while twenty (67%) are Class II sources. When corrected for possible selection effects due to extinction, (see Section 4), we predict that only 26% (10) of the sources in this luminosity range are Class I while 73% (28) are Class II. In contrast, Class I sources clearly dominate the population of sources in the adjacent, intermediate luminosity bins (i.e., $5.6\ L_\odot > L''(\mathrm{obs}) < 56\ L_\odot$), where 82% of the sources are Class I (i.e., 9 Class I objects compared to 1 Class II source and 1 Class IIID source). Expressed

in another way, of the 30 Class II sources with well determined luminosities (including the Class IID objects) only 1 (or 3% of the entire Class II population) has a luminosity in excess of $5.6\ L_\odot$. In contrast, 9 of the 24 Class I sources or 33% of the entire Class I population have luminosities in excess of $5.6\ L_\odot$.

There are two plausible explanations for this luminosity segregation. First, the Class I intermediate luminosity sources may be of similar mass to the Class II sources in the cloud but possess an additional source of energy which makes them systematically more luminous. If this is the case, our observations may provide important evidence for the existence of luminosity evolution between the Class I and Class II phases. The most likely source for the excess luminosity in the Class I phase would be accretion processes associated with protostellar evolution. Indeed, protostellar theory predicts that YSOs in the accretion (Class I) phase of their evolution will possess considerably higher luminosities than objects with similar mass on convective-radiative tracks on the HR diagram (i.e., Class II objects). Models by Stahler, Shu and Taam (1980) predict that a solar mass protostar will reach a peak luminosity of about $66\ L_\odot$ during the active accretion or infall phase of evolution. However, at the end of the accretion phase the luminosity will rapidly drop, falling to a value of about $6\ L_\odot$ at the time the young star first appears on the stellar birthline at the top of its convective track (Stahler 1983). Consequently, our observations may provide indirect but strong evidence of accretion around Class I sources and thus more compelling support for the protostellar interpretation of their nature. A second explanation of the observed segregation of Class I and II luminosities is that the Class I intermediate luminosity objects are stars of systematically higher mass (e.g., 2-4 $M_\odot$) than the Class II sources currently observed in the cloud.

In this case their Class I SEDs suggest that they are products of the most recent episodes of star formation in the cloud and that the ρ Oph cloud is forming stars sequentially in mass. At the present time it is not possible to distinguish between these two intriguing possibilities.

4) Relation to the Initial Luminosity Function

Of fundamental importance to the development of a theory of star formation is understanding the origin of the Initial Mass Function (IMF). Salpeter (1955) showed that the observed luminosity function of field stars, upon correction for stellar evolution, could be used to derive the original frequency distribution of stellar masses produced by the star formation process in interstellar clouds. Salpeter's work as well as many subsequent studies (e.g., Miller and Scalo, 1979; Scalo, 1986) have indicated that the IMF can be described by a power law with a negative spectral index. However, it has never been clear from existing observations whether or not the IMF is universal either temporally or spatially in the galaxy. It is of great interest to know, for example, if the initial mass functions of stellar populations formed in molecular clouds vary between different clouds or even from place to place within a given star forming cloud. In principle, constructing the luminosity function of the embedded population of an active star forming region is the most direct way to determine the original stellar mass function of a cloud and investigate the history of how the IMF is assembled.

The empirical luminosity function for the Ophiuchus cluster shown in Fig. 5 represents the first well determined luminosity function of a young embedded population of YSOs to be produced for an individual molecular cloud. It is therefore useful to investigate its relationship to the field IMF. As a first step we compare the empirical luminosity function of the embedded cluster

with the Initial Luminosity Function (ILF) corresponding to the IMF. To do this we have drawn the ILF for field stars in Figure 5. Here the ILF has been normalized to the number of YSOs observed to be in the $-0.25 < \log L''$ (obs) > 0.75 luminosity range (16 sources with upper limits are not included in this normalization). Taken at face value there are no statistically significant departures between the two sets of data. However, this is not necessarily very meaningful since the empirical luminosity function is incompletely sampled at low luminosities and, more significantly, a substantial adjustment to the observed luminosities must be made to account for luminosity evolution before direct comparison with the ILF can be appropriately made. This is because the ILF is derived from a mass-luminosity relation pertinent to hydrogen burning stars on the zero-age main sequence . The YSOs in Ophiuchus, on the other hand, are either pre-main sequence stars or protostars which derive their luminous energy from more exotic processes such as quasi-static gravitational contraction, deuterium burning, infall and/or accretion. For such objects there exists no clear cut mass-luminosity relation and no straightforward way to use the ILF to derive an initial mass function with any detail.

Nonetheless, it is possible to correct crudely the empirical luminosity function both for incomplete sampling and evolution. First we consider the incompleteness question. Based upon studies of the infrared colors of 1 $L_\odot$ T Tauri stars FN Tau, IQ Tau, HN Tau, DP Tau and GM Aur (Cohen and Kuhi 1979, Rydgren et al. 1984, Rucinski 1985), we have determined that a 1 $L_\odot$ T Tauri star with no extinction at a distance of 160 pc will have an apparent K magnitude of about 8.2 (0.33 Jy) and a 2-12 μm color temperature of 1000 K. Our typical T Tauri star has a spectral index of −0.65. Despite the fact that the 12 μm extinction due to dust is about one-third that at 2 μm (Rieke and Lebofsky 1985), the depth of the cloud layer which is completely sampled by IRAS at 12 μm for Class II objects is similar to that for 2 μm surveys with K-12 mag in unconfused regions (A_V = 35-40 mag). However, for regions of high source density, only the outer ~5-10 mag of the cloud is sampled by IRAS at 12 μm. The confusion in the 12 μm data would not be a serious problem if combined with sensitive 2 μm observations but, at present, only about half of the high extinction core has been surveyed to K=12 mag (Wilking and Lada 1983). Hence, a conservative correction to the observed luminosity function would involve doubling the number of Class II objects in the high extinction core (A_V>40 mag) which lie in the -0.25<log L"(obs)<0.75 range (8 objects). No such correction is necessary for 1 $L_\odot$ Class I objects because the presence of hot circumstellar dust increases the visibility of these embedded stars. For example, an object with a spectral index of a=1 which has an apparent magnitude of K=8.2 mag at the surface of the cloud would be detected in the coadded 12 μm data even if obscured by 90 mag of extinction.

Correcting for the number of Class II objects hidden by extinction in the cloud core results in a luminosity function which deviates from an appropriately renormalized ILF at intermediate luminositites (i.e., 5.6 $L_\odot$ < L < 100 $L_\odot$) by 2.5 standard deviations from what would be expected by Poisson noise. This is probably not a statistically significant deviation. In earlier studies of the ρ Oph luminosity function, LW argued for a more significant deficit of intermediate mass stars. However, our IRAS observations suggest that LW overestimated (by about 50%) the number of undetected stars at low luminosities. This was partly because they did not have enough long wavelength data to properly account for the variation in source detectability due to SED shape.

To make a crude estimate of the adjustment to the observed luminosity function likely to result from source evolution to the main sequence requires that we accept the connection between the morphology of the SED and an object's

evolutionary state (ALS, Section IVA). We also need to draw upon the results of protostar theory for the luminosity evolution of a PMS object. For example, Stahler, Shu, and Taam (1980) predict that as a 1 $M_\odot$ protostar approaches the ZAMS, it will experience a more dramatic drop in luminosity (by a factor of 10) relative to its more evolved T Tauri counterpart. Hence, we can simulate PMS evolution in Fig. 5 if we assume Class I objects at intermediate luminosity are 1$M_\odot$ protostars and allow them to "evolve" two luminosity bins to the left (a drop of a factor of 10) relative to the Class II objects.

The results of this simulation are not shown here but the luminosity function of the embedded cluster departs from the ILF (after appropriate renormalization to the larger low luminosity population) in what appears to be a statistically significant way at intermediate luminosities. Only seven objects with L > 5.6 $L_\odot$ remain after the correction for source (PMS) evolution, where 24 would be expected from the ILF and this is 3.5 standard deviations from what is expected from Poisson noise. This deficiency arises because the luminosity segregation of SED classes discussed in Section 3. Both the corrections for evolution and incomplete sampling suggest that the mass function of stars already produced in the cloud core deviates from the IMF at intermediate luminosities. Because our knowledge of the true natures and evolutionary histories of the embedded sources is uncertain, it is difficult to know how much significance to attach to this result. It is interesting to note however, that if real, this result suggests that the cluster which ultimately emerges from the cloud will have a mass function similar to the IMF only if future episodes of star formation favor the production of intermediate mass stars. We note that the conclusion that stars in the ρ Oph cloud core are forming sequentially with mass also results if we assume that the intermediate luminosity Class I sources are stars of intermediate mass and no luminosity evolution occurs (see Section 3).

Our observations have produced the first direct measurement of the actual initial luminosity function of an embedded population of young stellar objects. Such observations are potentially powerful for investigating the origin and development of the IMF. However, at the present time interpretation of the results is limited by uncertain knowledge of the nature and evolutionary histories of YSOs. It would be of great interest to assemble a calometric luminosity function for the embedded population of another nearby dark cloud for comparison with the results of this paper. Such a comparison would have distinct advantages over studies of the luminosity function of a single embedded population. For example, statistically significant differences between the luminosity functions of the embedded populations of different clouds would indicate that the question of the origin and development of the IMF is indeed accessible to observational investigation.

V. Summary

We have analysed high sensitivity IRAS data over a 4.3 pc^2 area of the central cloud in the Ophiuchus complex. These data have been combined with near-infrared and Hα surveys to investigate the nature of the dust-embedded cluster. The major results of this study are:

1) The IRAS data have enabled us to obtain a more complete and representative sample of the embedded population. We have associated 44 IRAS 12 μm sources with their optical/near-infrared counterparts. As a result, a total of 78 cluster members have now been firmly identified.

2) The IRAS observations show evidence for extended mid-infrared emission on size scales anywhere from 6 arcsec to tens of arcminutes. The extended emission most likely arises from either non-equilibrium heating of small dust grains or unresolved multiple sources.

3) Spectral energy distributions were constructed for 53 embedded objects and classified by their spectral index from 2.2-25 μm. The continuous distribution of SED shapes from heavily obscured (Class I) objects to T Tauri (Class II) stars suggests this variation represents a quasi-continuous evolutionary sequence, providing support for an idea already advanced by Adams, Lada, and Shu (1987) based upon theoretical models for the emergent flux from YSOs. From our data, we are able to estimate crudely that the duration of the accretion phase for Class I objects is 1-4 x 10^5 years and the mass accretion rate is 2.5-10 x 10^{-6} $M_\odot$/yr for a 1 $M_\odot$ star. In addition, the duration of star formation in the central cloud of the Ophiuchus complex is estimated to be between 1.5 and 3.5 million years.

4) Observed luminosities for 74 embedded objects have been determined by integrating their SED over the observed wavelength interval and including a correction which extrapolates the SED to infinite wavelength. We estimate that these observed luminosities are within a factor of two of the true bolometric luminosities.

5) The luminosities of the YSOs are segregated by their SED shapes. In particular, Class I objects are found to dominate at intermediate luminosities. Either these stars undergo luminosity evolution as they progress from Class I to Class II objects or stars in the cloud are being formed sequentially in mass.

6) Comparison of the observed luminosity function with the field star Initial Luminosity Function suggests that stars have formed in the cloud with a relative deficiency of intermediate mass objects. However, uncertainties concerning both the true natures of the embedded sources and their evolutionary histories renders this interpretation open to question.

7) Our results have enabled an improved estimate for the star formation

efficiency. We find that SFE > 22% for the ρ Oph core. This, coupled with our estimate for the duration of star formation in the cloud, suggests that star-forming activity has occurred in a relatively efficient burst rather than as a more gradual process.

ACKNOWLEDGEMENTS

We would like to thank Chris Walker for helping with the IRTF observations and Jim Blackwell for assisting with the data analysis. This research was supported in part under NASA's IRAS Data Analysis Program funded through the Jet Propulsion Laboratory. B.A.W. gratefully acknowledges partial support from a University of Missouri-St. Louis Summer Research Fellowship and Weldon Spring Award.

Appendix A

Classification of Stars and Infrared Sources Toward the ρ Oph Cloud

We have attempted to classify 122 stars and 2 μm sources observed toward the main molecular cloud of ρ Ophiuchi complex. The boundaries of the cloud are defined by the contour of ^{13}CO emission where $T_R^*(^{13}CO,\ 1\rightarrow 0)$ = 6 K (Loren, 1987). Figure A1 presents a flow chart tracing the various selection criteria applied to each star or infrared source to determine its nature: association member (A), field star (F), or unclassified object (U). As shown in Fig. A1, a major discriminator is the slope of the spectral energy distribution between 2.2 μm and 25 μm. We have adopted the definition of the spectral index after Lada (1987) as

$$a = \frac{d \log (\lambda F_\lambda)}{d \log \lambda} .$$

To compute "a", we have used the slope between 2.2 μm and the longest observed wavelength between 10 and 25 μm. By considering a group of ten field stars in the vicinity of the ρ Oph cloud, we have empirically determined that a spectral index of "a" >-1.2 is characteristic of an association member. The ten field stars had been previously identified as K or M giants and observed in the infrared (Elias 1978). Most of these stars were found to be 12 μm or 25 μm sources in the IRAS Point Source Catalog (1985). Their energy distributions, shown in Fig. A2 (except for VSSG16) along with that of an unreddened 2000 K blackbody, display little evidence for luminous circumstellar dust. The average value for the spectral index of these stars is -2.0 with a sample standard deviation of 0.4. For our study, we have conservatively chosen a threshold of value "a" for association members which is two sample standard deviations away from this mean.

Two final selection criteria were applied to stars which had no mid-infrared photometry and estimate of "a". First, we compared the maximum visual extinction toward each star, as determined from the (H-K) color, to the total cloud extinction in that direction as estimated from the $C^{18}O$ column density (Wilking and Lada 1983). The A_V estimate for the star is an upper limit because it assumes there is no infrared excess at H or K and that the intrinsic colors can be ignored relative to the much larger observed colors. The latter estimate of total cloud extinction presumes the cloud is not clumpy within the one arcmin CO beam (which is a reasonable assumption based upon the study of Frerking, Langer, and Wilson 1982) but may have a factor of two uncertainty. To be conservative, we allowed a source with a maximum extinction, A_V = 12(H-K), which is less than half that of the total cloud, $A_V(C^{18}O)$, to be embedded in the cloud. Those stars which fail this test and have no infrared excess, as measured by the ratio of the (K-L) to (H-K) colors, are either field stars or post T Tauri stars. Spectrophotometry of six of the brighter 2 μm sources has been obtained (Elias 1978); the 2.3 μm CO absorption is observed in five objects indicating they are background K or M giants.

The results of this classification scheme are presented in Tables A1, A2, and A3 for association members, field stars and unidentified objects, respectively. Three of the sources in Table A1 (which also appear in Table 2) have been classified as association members solely on the basis of their coincidence with IRAS emission and are denoted by colons. Further photometric observations are necessary to confirm whether they are the actual luminosity source of the IRAS emission. Each table presents the aliases which have accumulated for each source over years of study. A key to the abbreviations used for cross-references is given in the footnote to Table A1. The distribution of the 78 association members in the ρ Oph cloud is shown in Fig. A3.

Appendix B

The Star Formation Efficiency Revisited

We can use the completely-sampled IRAS coadded survey data of the ρ Oph cloud to re-evaluate the star formation efficiency in the core region. The star formation efficiency is defined as: $SFE = M_{stars}/(M_{stars} + M_{gas})$. Although our approach to estimate the SFE utilizing the IRAS results is somewhat different from LW, a similar value is obtained. We consider here only the cluster members which lie within the $A_V = 50$ mag contour which contains about 290 $M_\odot$ of molecular gas (Wilking and Lada 1983).

To estimate the total mass of YSOs with $M > 1\ M_\odot$, we distinguish between Class I and Class II objects in our sample. Following the same lines of argument as those in Section IVB, we estimate that for $L > 1\ L_\odot$, we are completely sampled throughout the depth of the core with the coadded survey data for Class I objects. But for Class II objects, the IRAS survey has a similar sensitivity as existing 2 μm surveys and only about one-half of the depth of the core (A_V = 35-40 mag) has been fully sampled for $L > 1\ L_\odot$. Assuming that the embedded objects are uniformly distributed throughout the cloud, we double the observed Class II population to obtain a more representative sample over the entire depth of the core. Thus, our estimate of the cluster mass for $L > 0.56\ L_\odot$ is 39 $M_\odot$ and includes Source 1 (~9 $M_\odot$), 14 observed Class I objects (~1 $M_\odot$ each), and 8 observed Class II objects times 2 (~1 $M_\odot$ each).

We rely on 2 μm surveys to estimate the total mass of objects <1 $M_\odot$ since the IRAS data becomes confused for low luminosity sources. There are 9 Class I or Class II sources with $L < 0.56\ L_\odot$ and $K < 12$ mag which lie in the area surveyed by Wilking and Lada (1983). Since this region includes only half of the area encompassed by the 50 mag contour, we anticipate that future 2 μm

surveys of similar sensitivity will reveal an additional 9 low-luminosity sources. Based upon the study of T Tauri stars by Cohen and Kuhi (1979), we estimate that a 0.25 $L_\odot$ object at the front surface of the cloud will have an apparent magnitude at K of 9.5 mag. Therefore, a 2 μm survey with a sensitivity of K = 12 mag completely samples the outer 25 mag layer for objects with $L > 0.25\ L_\odot$. Assuming these objects have an average mass of 0.5 $M_\odot$, we would expect about 27 $M_\odot$ (54 objects) in the low-luminosity population for the entire core.

The final population of objects which must be accounted for in the cloud are the embedded Class III sources. As we discuss in Sec. IVA, the IRAS observations are insensitive to these objects. Using the 2 μm survey of Wilking and Lada, we estimate there are roughly equal numbers of Class II and Class III objects embedded in the cloud. Thus a total of sixteen 1 $M_\odot$ Class III objects are expected throughout the core.

As a result, the total stellar mass of the cluster in the core region is about 82 $M_\odot$ and the star formation efficiency 22%. Within the uncertainties of the estimate, this value is consistent with that of 25% calculated by LW. One uncertainty is the mass of molecular gas computed from $C^{18}O$ column densities. But we have minimized this uncertainty by correcting for the association members hidden by extinction; an increase in the computed hydrogen column densities would be compensated for by an increased correction for this unseen population. Other major uncertainties which include cold sources missed due to confusion in the IRAS data and the presence of binaries (e.g., SR12, Simon et al. 1987), will serve to raise the SFE when properly accounted for. In this sense, we view the value of 22% as a lower limit.

TABLE 1

IRAS SOURCES IN THE ρ OPHIUCHI CLOUD

IRAS Source[a] (1)	R.A.(1950) (2)	Dec.(1950) (3)	Flux Density[b] (Jy) 12 μm (4)	25 μm (5)	60 μm (6)	100 μm (7)	FWHP (arcsec)[c] (8)	2 μm Survey? (9)	IRTF 2μm Sources[d] (10)	IRTF(12μm)/IRAS(12μm)[e] (11)	SED? (12)
1	$16^h23^m51^s.1$	−24°14′.6	>8	>0.2	>7		ext	yes	(f)	–	no
2	16 23 42.7	−24 27.9	3.7	>11	>40		unres	no	WL12	0.76	yes
3	16 23 57.2	−24 38.7	3.5	6.3	11		unres	no	SR24N+S	0.49	yes
4	16 23 59.1	−24 28.2	6.0	16	260	790	unres	yes	WL22	0.52	yes
5	16 24 02.2	−24 30.6	19	<40	202		unres	no	WL16	0.39	yes
6	16 24 05.0	−24 21.8	3.8				140	yes	WL1	0.03	yes
7	16 24 08.0	−24 30.5	31	82	230	590	unres	no	EL29	0.97	yes
8	16 24 09.1	−24 12.4	3.0	26	43		unres	no	SR21	0.55	yes
9	16 24 10.0	−24 26.2	1.2				140	yes	WL9	<0.04	no
10	16 24 10.0	−24 18.8	5.3				205	yes	IRS34	0.04	no
									IRS30,32,33,36	<0.18	
11	16 24 11.7	−24 31.8	1.1	10	54		unres	no	WL19+20	0.34	yes
12	16 24 16.8	−24 22.0	1.6	12	85	190	unres	yes	IRS37	0.19	yes
									WL3,WL4,WL5	<0.24	
13	16 24 21.3	−24 34.9	3.5	6.2			unres	yes	IRS42	0.34	yes
14	16 24 20.4	−24 23.0	2.7	8.9			unres	no	WL6	0.80	yes
15	16 24 26.4	−24 34.0	3.2	27	136		unres	yes	IRS43	0.77	yes
16	16 24 28.1	−24 32.7	7.2	47	136		unres	yes	IRS44	0.60	yes
									IRS46	0.11	
17	16 24 29.6	−24 20.8	2.8	2.8			unres	no	VSSG17+18	0.72	yes
18	16 24 32.6	−24 34.3	3.4				unres	no	no candidates	–	no
19	16 22 37.0	−24 08.9	2.4	0.97			unres	yes	IRS2	0.07	no
20	16 22 42.5	−24 20.5	18	100	(g)	(g)	unres	yes	IRS7	–	no
21	16 22 43.5	−24 11.8	12	11	110	220	unres	yes	IRS8	–	no
22	16 22 45.7	−24 18.7	12	(g)			unres	no	no candidates	–	no
23	16 22 46.0	−24 24.7	0.41				unres	yes	IRS9	<0.1	yes
24	16 22 55.0	−24 23.8	0.22				unres	yes	GSS20(IRS13)	<0.3	yes
									IRS11	–	
25	16 22 56.0	−24 13.9	10	13			unres	no	SR4(IRS12)	0.08	yes
26	16 23 00.0	−24 15.8	88	62			210	no	GSS23	–	no
27	16 23 05.0	−24 36.3	0.70	0.28			unres	no	EL15	1.4	yes
28	16 23 07.5	−24 27.4	130	130	1100	1400	180	no	SR3	0.002	yes
29	16 23 15.1	−24 06.2	0.11				unres	no	no candidates	–	no
30	16 23 16.0	−24 32.9	0.43	1.2			unres	no	no candidates	–	no
31	16 23 20.0	−24 21.7	3.4	5.6			unres	no	VSSG1	0.23	yes
32	16 23 21.5	−24 09.5	2.4	3.3			unres	no	EL24	1.0	yes
33	16 23 21.6	−24 03.5	1.5	5.7			90	no	no candidates	–	no
34	16 23 25.0	−24 36.9	5.1	10.2			100	no	DoAr25	–	no
35	16 23 28.0	−24 24.4	1.1	0.60			unres	yes	IRS14	<0.08	no
36	16 23 30.3	−24 16.7	140	320	3400	5700	110	no	Source1	0.003	yes
									VSSG27		
37	16 23 39.5	−24 05.3	0.60	1.3			unres	no	VSS27±α		yes
38	16 23 40.0	−24 24.5	0.44	0.89			unres	yes	WL7(IRS17)	0.19	yes
39	16 23 41.0	−24 09.5	0.60	0.17			unres	yes	VSSG11(IRS19)	<0.14	yes
40	16 23 50.0	−24 17.5	6.3	45	(h)	(h)	unres	yes	no candidates	–	no
41	16 23 51.5	−24 02.3	1.8	1.8			135	no	no candidates	–	no
42	16 24 04.9	−24 07.5	0.15	0.91			unres	no	no candidates	–	no
43	16 24 10.0	−24 33.9	0.71	2.9			unres	no	no candidates	–	no
44	16 24 26.2	−24 10.5	<0.09		3.6	40	unres	no	ROX23, VSSG22?	–	no
45	16 24 36.0	−24 36.4	1.0	3.0	11		unres	yes	IRS51	1.4	yes
46	16 24 37.5	−24 24.0	8.1	39	94		unres	yes	IRS48	0.74	yes
									IRS50		
47	16 24 37.5	−24 30.2	0.28	0.88			unres	yes	IRS49	2.0	yes
48	16 24 39.7	−24 05.2	0.94	0.63			unres	no	no candidates	–	no
49	16 24 40.5	−24 15.4	0.60	1.5	14		unres	no	SR9(IRS52)	0.93	yes
50	16 24 42.0	−24 18.5	0.14	0.41	1.0		unres	no	no candidates	–	no
51	16 24 47.5	−24 33.0	0.38	0.47			unres	yes	ROX31?	–	no
52	16 24 47.7	−24 25.0	6.5	21	83	74	unres	yes	IRS54	2.3	yes
53	16 24 48.0	−24 19.2	0.40				unres	no	VSSG14	0.16	yes
54	16 24 48.2	−24 41.4	0.2(i)				unres	yes	IRS56	<0.5	no
55	16 24 57.0	−24 16.3	0.2	0.18			unres	no	no candidates	–	no
56	16 24 59.0	−24 19.7	0.42				80	no	VSSG16(IRS58)	0.24	
									SR10±α	–	yes
57	16 25 03.5	−24 14.0	0.83	3.4	27	42	60	yes	no candidates	–	no
58	16 25 17.4	−24 30.5	0.12	0.22	4.0	54	unres	no	Hα60	–	no
59	16 25 24.6	−24 14.0	0.34	0.26	11		unres	no	no candidates	–	no
60	16 25 24.6	−24 16.1	0.17	0.27			unres	no	SR20±α	–	yes
61	16 25 41.9	−24 09.1	0.19				unres	no	no candidates	–	no
62	16 25 56.0	−24 15.7	0.90	0.60	4.6		unres	no	no candidates	–	no
63	16 26 13.0	−24 36.5	0.17				unres	no	no candidates	–	no
64	16 26 22.2	−24 07.5	0.24	0.35			unres	no	no candidates	–	no

Notes to Table 1 -

(a) IRAS sources 1-18 were previously presented in Paper I and were referred to as YLW 1-18 by Wilking, Schwartz, and Blackwell (1987) while IRAS sources 19-64 were referred to as WLY 1-46.

(b) Photometric uncertainties are ±15% for isolated point sources and as high as ±30% for heavily confused sources. Upper limits for 12 μm fluxes are 3σ.

(c) Inscan FWHP at 12 μm in arcseconds. "Unres" indicates source is unresolved (< 45").

(d) Near-infrared sources within 20" in-scan (dec.) and 45" cross-scan (r.a.) of IRAS position except when noted. Source names followed by "$\pm\alpha$" are 70-90" away from the IRAS position in r.a. but within 4" in dec. Sources followed by "?" lie just outside our search area in both r.a. and dec. Source names are from Table 2 (IRS) or from Grasdalen, Strom, and Strom (GSS,1973), Struve and Rudkjobing (SR,1949), Elias (EL,1978), Vrba et al. (VSSG,1975), Dolidze and Arakeylan (DoAr,1959), Wilking and Lada (WL,1983), Wilking, Schwartz, and Blackwell (Hα,1987), Vrba, Strom, and Strom (VSS,1976), and Montmerle et al. (ROX,1983).

(e) Ratio of ground-based to IRAS 12 μm flux densities. An extrapolation of ground-based 10 μm measurement is made using slope of 2-10 μm energy distribution.

(f) Source appears at edge of high resolution AO and is apparently part of the extended 12 μm emission from the 2 μm Source 1.

(g) Source confused in emission excited by HD147889.

(h) Source confused in emission excited by 2μm Source 1.

(i) Source badly confused at edge of extended plateau of emission.

Table 2

Observational Results for IRTF Sources

IRS	Other Names(a) (1)	R.A.(1950) (2)	DEC.(1950) (3)	Flux in Magnitudes(b) 1.25 μm (4)	1.6 μm (5)	2.2 μm (6)	3.4 μm (7)	4.8 μm (8)	10 μm (9)	20 μm (10)	Vis.(c) Star? (11)	A(v) = 12(H-K)(d) (12)	A(v) (C18O)(e) (13)	A/F(f) (14)	Aperture J-L (") (15)	Aperture M-Q (") (16)	Date of Obs. (17) 7/84	5/85	6/86
1	EL11,GSS15	$16^{h}22^{m}34.0^{s}$	$-24^{\circ}27'13''$						>6.2		yes	12.0		F		5.5			X
2		16 22 35.5	-24 8 52	10.37	8.88	8.28	7.85	>7.7	5.8		yes	7.2		A	7.5	5.5			X
									0.2										
3		16 22 38.0	-24 19 46	11.55	9.77	8.79	7.68		6.3	>3.0	yes	11.8		U	7.5	5.5			X
									0.2										
4		16 22 38.7	-24 10 17	14.43	12.69	11.97					no	8.6		U	7.5				X
				0.09	0.04														
5		16 22 39.3	-24 19 29		13.25	12.28	11.6				no	11.6		U	7.5				X
							0.2												
6		16 22 39.5	-24 9 58		13.21	12.33	>10.9				no	10.6		U	7.5				X
					0.04														
7		16 22 40.7	-24 20 23		13.62	12.79	11.6				no	10.0		A:	7.5				X
							0.1												
8		16 22 46.3	-24 11 43	12.87	10.59	9.64	9.0				no	11.4		A:	5.5			X	
							0.1												
9		16 22 47.4	-24 24 50	13.13	10.57	9.42	8.65	>8.6	>7.2		no	13.8		A	7.5	5.5			X
10	VSS23,ROX4	16 22 48.8	-24 32 27						>6.7		yes	6.0		A		5.5			X
11		16 22 54.5	-24 23 28		10.42	9.81		>8.2			no	7.3		U	7.5	5.5			X
12	SR4(TT),ROX6	16 22 54.8	-24 14 1						4.09	1.9	yes	7.6		A		5.5			X
13	GSS20,ROX7	16 22 55.9	-24 23 43	10.33	8.85	8.29	8.0	7.9	>6.7		yes	6.7		A	7.5	5.5			X
								0.2											
14		16 23 29.3	-24 24 20	15.29	12.27	10.9	9.93		>6.7		no	16.4	25	A:	7.5	7.5	X		
15		16 23 30.1	-24 24 56		14.63	13.36	11.8		>6.7		no	15.2	32	A	7.5	7.5	X		
							0.2												
16		16 23 39.1	-24 24 6			13.2	11.7		>7.0		no		50	U	7.5	7.5	X		
							0.2												
17	WL7	16 23 40.5	-24 24 18			11.13	9.03		6.6	>2.0	no	21.7	50	A	7.5	5.5-7.5	X		X
18		16 23 41.2	-24 17 44		15.7	13.33	12.4				no	28.4	49	U	5.5			X	
					0.1		0.2												
19	VSSG11,ROXC9	16 23 42.3	-24 9 48	13.1	10.55	9.45	8.62		>6.6		no	13.2	22	A	5.5	5.5		X	X
20	YLW1A	16 23 49.7	-24 14 7		11.51	10.26	9.52		>7.0		no	15.0	16	U	5.5	7.5	X		
21	VSSG6,ROXC12	16 23 52.3	-24 15 44	14.67	11.41	9.81	8.87				no	19.2	24	U	7.5				X
22	VSSG7	16 23 53.9	-24 13 45		11.76	9.82	8.54		>6.7		no	23.3	23	U	5.5	7.5	X		
23	WL21	16 23 55.5	-24 28 55	19.6(g)	15.19(g)	12.78	11.13	>8.1	>6.8	>2.7	no	29.2	75	A	7.5	7.5	X		
24	SR24N(TT)	16 23 56.4	-24 38 48						3.91	>2.7	yes			A		5.5		X	
25	SR24S(TT)	16 23 56.5	-24 38 55						4.35	1.8	yes			A		5.5		X	
26	YLW1C	16 23 56.9	-24 14 47	16.4	13.02	11.36	9.99	>8.4	>7.0		no	19.9	23	U	5.5	5.5		X	X
				0.1															

Table 2 (con't)

Observational Results for IRTF Sources

IRS	Other Names(a) (1)	R.A.(1950) (2)	DEC.(1950) (3)	Flux in Magnitudes(b) 1.25 µm (4)	1.6 µm (5)	2.2 µm (6)	3.4 µm (7)	4.8 µm (8)	10 µm (9)	20 µm (10)	Vis.(c) Star? (11)	A(v) = 12(H-K)(d) (12)	A(v) (C18O)(e) (13)	A/F(f) (14)	Aperture J-L (") (15)	Aperture M-Q (") (16)	Date of Obs. 7/84 (17)	5/85	6/86
27	WL22	$16^h 23^m 57^s.3$	-24°28'15"		>16.7	14.47	7.8	5.4	3.77	1.8	no		84	A	5.5-7.5	7.5	X	X	
28	VSSG8	16 24 0.1	-24 14 54	14.13	10.81	9.3	8.34	8.2	>5.8		no	18.1	23	U	7.5	5.5			X
				0.06				0.3											
29	WL1	16 24 2.4	-24 21 46	16.7	12.65	10.62	8.78		6.2	>3.3	no	24.4	46	A	5.5	5.5		X	X
				0.2					0.2										
30	YLW10A	16 24 4.1	-24 19 37		13.21	10.87	9.44				no	28.1	44	U	5.5			X	
31	WL9	16 24 8.5	-24 26 39			11.97	10.72		>7.2		no	23.2	75	A	7.5	7.5	X		
32		16 24 10.1	-24 16 59	14.37	11.5	10.06	9.17	7.9	>4.1		no	17.3	24	U	7.5	5.5			X
				0.05				0.25											
32b		16 24 11.8	-24 36 49			10.1					no		40	U					
						0.2													
33		16 24 12.8	-24 20 4		15.3	12.15	10.2	>8.1	>6.6		no	37.8	41	U	7.5	5.5			X
					0.1														
34	YLW10B	16 24 13.6	-24 19 58		13.08	10.43	8.4	7.1	5.7	>2.7	no	31.8	41	A	5.5	5.5		X	X
								0.15											
35		16 24 13.8	-24 24 12		16.6	12.86	10.54		>7.0		no	44.9	64	U	7.5	7.5	X		
					0.2														
36	YLW10C	16 24 13.9	-24 18 33		15.6	12.95	11.12				no	31.8	39	U	5.5			X	
					0.1														
37	YLW12A	16 24 15.9	-24 22 14	>16.8	13.99	11.48	8.77		5.6	>2.6	no	30.1	55	A	5.5	7.5	X		
38	WL5	16 24 16.5	-24 22 9		14.26	10.38	7.92		>7.4		no	46.6	55	U	5.5	7.5	X		
39	WL4	16 24 16.8	-24 22 23		11.37	9.59	8.21				no	21.4	55	A	5.5		X		
40	SR12(TT),ROX21	16 24 17.5	-24 34 59	9.54	8.67	8.46	8.22	8.5	>7.1		yes	2.5	60	A	5.5	5.5		X	X
								0.3											
41	WL3	16 24 17.6	-24 22 0		14.17	11.2	8.8		6.8	>2.0	no	35.6	55	A	5.5	7.5	X		
									0.3										
42	YLW13B,ROX21	16 24 19.3	-24 35 3	15.7	11.26	8.39	5.88		3.91	>2.4	no	34.4	71	A	5.5	5.5		X	
				0.05															
43	YLW15A	16 24 24.9	-24 34 9		13.61	9.96	6.85		3.34	0.27	no	43.8	80	A	7.5	7.5	X		
44	YLW16A	16 24 26.0	-24 32 52	>16.8	13.51	9.84	6.68		2.33	-1.23	no	44.0	68	A	7.5	7.5		X	X
45	VSSG18	16 24 26.7	-24 20 40						5.1	>2.7	no	28.8	48	A		5.5			X
46	YLW16B	16 24 27.4	-24 32 36	16.9	12.95	10.17	7.63		4.2	1.7	no	33.4	68	A	5.5	7.5	X	X	
				0.15															
47	VSSG17	16 24 28.8	-24 21 4						3.53	1.87	no	31.1	48	A		5.5	X		
48		16 24 35.5	-24 23 55	10.78	8.6	7.4	5.91		2.2	-0.98	yes	14.4	34	A	5.5-7.5	7.5	X	X	
49	ROXC20	16 24 36.4	-24 30 18	11.62	9.43	8.37	7.24		4.63		no	12.7	35	A	7.5	7.5	X		
50		16 24 36.4	-24 24 1		10.57	9.67	9.07		>6.8		no	10.8	34	A	7.5	7.5	X		

Table 2 (con't)

Observational Results for IRTF Sources

IRS	Other Names(a) (1)	R.A.(1950) (2)	DEC.(1950) (3)	Flux in Magnitudes(b) 1.25 µm (4)	1.6 µm (5)	2.2 µm (6)	3.4 µm (7)	4.8 µm (8)	10 µm (9)	20 µm (10)	Vis.(c) Star? (11)	A(v) = 12(H-K)(d) (12)	A(v) (C18O)(e) (13)	A/F(f) (14)	Aperture J-L (") (15)	Aperture M-Q (") (16)	Date of Obs. (17) 7/84	5/85	6/86
51		$16^h24^m37\overset{s}{.}6$	−24°36'35"	>17.7	12.42	8.95	6.15		3.78	1.6 0.25	no	41.6	45	A	5.5	5.5		X	
52	SR9(TT),ROX29	16 24 38.8	−24 15 24						4.49	2.9 0.3	yes	7.2	5	A		5.5		X	
53		16 24 41.6	−24 36 28		13.72	11.21	9.71		>7.0		no	30.1	32	U	7.5	7.5	X		
54		16 24 50.0	−24 25 5	13.95	10.78	8.2	4.73	3.0 0.1	1.41	−1.02	no	31.0	29	A	5.5	5.5		X	X
55	ROX31	16 24 50.3	−24 34 10	10.15	8.7	8.21	7.78	>8.9	>7.2		yes	5.9	30	A	7.5	5.5			X
56		16 24 50.8	−24 41 16	11.85	9.39	8.37	7.73		>6.2		no	12.2		U	7.5	5.5			X
57		16 24 58.3	−24 15 20			13.38	12.4 0.3				no			U	7.5				X
58	VSSG16	16 25 2.1	−24 19 54			6.49	6.17	6.4	6.1		yes	7.1		F	7.5	5.5			X

Notes to Table 2 -

(a) References for source names are same as those in Table 1 with the addition of Young, Lada, and Wilking (YLW, 1986). T Tauri stars are denoted by 'TT'.

(b) Limits are 3σ upper limits.

(c) Optical counterparts as identified from the red POSS photograph (m< 20.0 mag).

(d) An upper limit to the visual extinction toward a YSO obtained assuming the intrinsic (H-K)=0.

(e) The total cloud extinction as estimated from the $C^{18}O$ column density (Wilking and Lada 1983).

(f) Classification of 2 µm source as association member (A), field star (F) or unclassified (U) as determined from criteria described in Appendix A.

(g) Photometry by Hyland (unpublished observations).

TABLE 3

SPECTRAL INDICES AND LUMINOSITIES

Association Member	Spectral Index a	$(2.2-\lambda_f)$	L(fir)	Luminosity ($L_\odot$) L'(obs)	$\lambda_i-\lambda_f$ (μm)	L"(obs)
HD147889	Class IIID		4500(a)			5500(b)
SOURCE 1	Class IIID		201	205	(.45-100)	1500(c)
SR3	Class IIID		69	92	(.36-100)	125(c)
EL29	0.70		21	34	(1.25-100)	48
WL22	3.0		17	19	(2.2-100)	38
GSS23	Class IIID		8	32	(.36-25)	25(c)
WL16	0.79		10	14	(1.25-60)	22
IRS44	1.7		8.8	10	(1.25-60)	16
IRS43	1.5		6.1	7.2	(1.6-60)	13
IRS48	0.65		6.2	9.2	(1.25-60)	13
IRS54	0.70		5.6	10	(1.25-100)	12
GSS30	1.2	(20 μm)		5.6	(1.25-20)	11
IRS37	1.7		3.5	6.1	(1.6-100)	11
SR21	Class IID		3.4	6.3	(.36-100)	7.0
SR4(TT)	Class IID		1.2	4.3	(.36-25)	5.5
DoAr25	0.23		0.80	4.1	(.65-25)	5.1
WL12	1.5		2.2	3.3	(1.6-60)	4.9
SR24S(TT)	-0.39		1.0	3.5	(1.25-60)	4.0(d)
GSS31	-0.50	(20 μm)		3.2	(.36-20)	3.7
EL24	-0.41		0.43	2.7	(.7-25)	3.2
SR9(TT)	-0.85		0.12	2.7	(.36-25)	2.8
IRS42	0.29		0.5	2.1	(1.25-25)	2.7
SOURCE 2	-0.68	(20 μm)		2.3	(.7-20)	2.5
VSSG1	0.05		0.36	2.2	(.9-25)	2.5
WL20	0.68		1.2	1.6	(1.25-60)	2.5(e)
WL19	0.68		1.2	1.6	(1.25-60)	2.5(e)
WL6	0.98		0.60	1.5	(1.6-25)	2.4
Hα60	Class IID?		0.60	0.81	(.65-100)	2.0:(f)
VSSG17	-0.05		0.45	1.6	(1.25-25)	1.8
WL1	1.8		0.40	1.0	(1.25-12)	1.8
SR20(TT)	-1.6		0.02	1.6	(.36-25)	1.7
IRS51	0.27		0.52	1.2	(1.25-60)	1.4
VSS27	-0.66		0.10	1.2	(.55-25)	1.3
IRS2	-0.52		0.18	1.1	(1.25-25)	1.2
SR24N(TT)	Class II					1.2(c)(d)
VSSG14	-1.3			1.1	(.45-12)	1.1
GSS28(TT)	-0.50	(10 μm)		0.94	(.36-10)	1.1
GSS29	-0.77	(10 μm)		0.60	(.45-10)	0.80
IRS46	0.66	(20 μm)		0.48	(1.25-20)	0.73
GSS26	-0.30	(20 μm)		0.60	(1.25-20)	0.70
SR12A(TT)	Class II					0.64(c)
SR10(TT)	-0.65	(12 μm)		0.55	(.36-12)	0.63
SR22(TT)	Class II					0.60(c)
IRS49	-0.53		0.06	0.48	(1.5-25)	0.56
GSS20	-1.2	(12 μm)		0.37	(1.25-12)	0.42
GSS39	-0.55	(12.5 μm)		0.32	(1.25-12.5)	0.40
VSSG27	-0.38	(12.5 μm)		0.32	(1.6-12.5)	0.36
VSSG11	-0.79			0.30	(1.25-25)	0.32
WL17	0.16	(12.5 μm)		0.25	(1.6-12.5)	0.32
WL10	-0.90	(10 μm)		0.25	(1.25-10)	0.30
IRS9	-0.20	(12 μm)		0.21	(1.25-12)	0.30
VSSG18	0.01	(10 μm)		0.20	(1.25-10)	0.28
WL7	0.52		0.0~~6~~7	0.14	(1.25-25)	0.23
WL4	-0.58	(10 μm)		0.16	(1.25-10)	0.18
IRS34	0.02	(10 μm)		0.13	(1.6-10)	0.18
SR12B	Class II					0.16(c)
WL2	-0.23	(10 μm)		0.08	(1.6-10)	0.10
WL3	0.24	(10 μm)		0.06	(1.6-10)	0.10
IRS50				<4.7	(1.6-25)	<9.0(g)
VSSG12				<1.8	(1.6-25)	<2.3
VSSG2				<1.2	(.7-25)	<1.6
WL11				<0.4	(1.6-25)	<0.9
WL14				<0.5	(1.6-25)	<0.9
WL21				<0.5	(1.25-25)	<0.9
VSSG25				<0.5	(.9-25)	<0.8
VSSG3				<0.5	(.9-25)	<0.6
IRS55				<0.4	(1.25-25)	<0.4
VSSG5				<0.2	(1.6-25)	<0.4
Hα37				<0.3	(.65-25)	<0.3
Hα63				<0.2	(.65-25)	<0.3
Hα49				<0.2	(.65-25)	<0.2
IRS15				<0.1	(1.6-25)	<0.2
VSSG22				<0.1	(1.6-25)	<0.1
WL9				<0.1	(1.6-25)	<0.1

TABLE 3 (con't)

Field/Unidentified Objects	a	$(2.2-\lambda_f)$
EL15	-1.9	
IRS56	-1.2:	(12 μm)
VSSG16	-2.6	(10 μm)
IRS3	-1.4	(10 μm)
WL8	-1.3	(10 μm)

Notes to Table 3:

(a) Young and Greene (1988).

(b) Luminosity for B2V star (Garrison 1967).

(c) For sources with estimate of A_v, bolometric luminosity was determined from dereddened energy distribution: GSS23 (Lada and Wilking 1984), SR24N, SR22 (Cohen and Kuhi 1979), and SR12A, SR12B (Simon et al. 1987).

(d) SR24S is most luminous of SR24 pair (see Table 2).

(e) WL19 and WL20 assumed to contribute equally to IRAS emission.

(f) Rough estimate of bolometric luminosity obtained by combining magnitude at 0.65 μm from red POSS print with IRAS flux densities.

(g) Sources with upper limits to luminosity were not detected by IRAS because they were confused or below detection limit. Upper limits to 12 and 25 μm flux density were determined from in-scan slices centered on the 2 μm positions.

TABLE A1

A Cross-Reference List of Rho Oph Cluster Members[1]

	R.A. (1950)	Dec(1950)	SR	GSS	VSSG	VSS	C1	EL	WL	ROX	Hα	IRAS/YLW	IRS	other
	h m s													
1	16 22 22.7	-24°22'55"	22				5				23			
2	16 22 22.8	-24 21 7	1	9			4	9						HD147889
3	16 22 35.5	-24 8 52										19	2	
4:	16 22 40.7	-24 20 23										20?	7	
5:	16 22 46.3	-24 11 43										21?	8	
6	16 22 47.4	-24 24 50										23	9	
7	16 22 54.8	-24 14 1	4				7	13		6	25	25	12	
8	16 22 55.9	-24 23 43		20						7		24	13	
9	16 23 1.7	-24 16 50		23		93	10	14		8		26		
10	16 23 7.7	-24 27 26	3	25		92	12	16				28		
11	16 23 9.0	-24 14 11		26										S26
12	16 23 14.8	-24 15 21			12									
13	16 23 15.5	-24 15 38		29			13	18						S28
14	16 23 15.8	-24 13 37		28			14	19		10	27			
15	16 23 17.5	-24 21 33			1		15	20				31		
16	16 23 19.9	-24 16 18		30				21						S29
17	16 23 21.7	-24 36 29				25				C3	29	34		DoAr25
18	16 23 22.0	-24 14 15		31			16	22		10	30			
19	16 23 22.6	-24 18 4		32			17	23		C6				S2
20	16 23 22.9	-24 9 29						24		C5	31	32		
21	16 23 28.7	-24 16 14			27							36		
22:	16 23 29.3	-24 24 20										35?	14	
23	16 23 30.1	-24 24 56											15	
24	16 23 32.8	-24 16 44		35		26	19	25		14		36		S1
25	16 23 39.4	-24 33 34									37			
26	16 23 40.5	-24 24 18							7			38	17	
27	16 23 41.5	-24 13 47		37	2		20	26		15				
28	16 23 42.3	-24 9 48			11					C9		39	19	
29	16 23 42.5	-24 28 4							12			2		
30	16 23 43.3	-24 16 24		39				27						
31	16 23 45.1	-24 5 17				27				16	38	37?		
32	16 23 46.8	-24 21 53							2					
33	16 23 47.0	-24 13 24			3		21			17				
34	16 23 52.0	-24 19 39			5					C11				
35	16 23 55.5	-24 28 55							21			4	23	
36	16 23 56.4	-24 38 48	24N					28		C13	41	3	24	
37	16 23 56.5	-24 38 55	24S					28		C13	42	3	25	

TABLE A1 (CON'T)

	R.A. (1950)	Dec(1950)	SR	GSS	VSSG	VSS	C1	EL	WL	ROX	Hα	IRAS/YLW	IRS	other
	h m s													
38	16 23 57.2	-24°29' 8"							14			4		
39	16 23 57.3	-24 28 15							22			4	27	
40	16 24 0.3	-24 30 44							16			5		
41	16 24 2.4	-24 21 46							1			6	29	
42	16 24 4.8	-24 31 33							17					
43	16 24 7.3	-24 27 35							10					
44	16 24 7.8	-24 30 33						29	15	C15		7		
45	16 24 8.5	-24 26 39							9			9	31	
46	16 24 8.9	-24 12 31	21		23	31	25	30		C14		8		
47	16 24 9.5	-24 28 7							11					
48	16 24 9.7	-24 31 49							19			11		
49	16 24 13.6	-24 19 58										10	34	
50	16 24 13.9	-24 31 59							20			11		
51	16 24 15.9	-24 22 14			26							12	37	
52	16 24 16.8	-24 22 23			26				4			12	39	
53	16 24 17.5	-24 34 59	12A							21			40	binary
54	16 24 17.5	-24 34 59	12B							21			40	
55	16 24 17.6	-24 22 0			26				3			12	41	
56	16 24 19.3	-24 35 3								21		13	42	
57	16 24 19.8	-24 23 8							6			14		
58	16 24 20.8	-24 11 24			22					23				
59	16 24 20.9	-24 41 27									49			
60	16 24 24.9	-24 34 9										15	43	
61	16 24 25.4	-24 24 34			25		27	31	13					
62	16 24 26.0	-24 32 52										16	44	
63	16 24 26.7	-24 20 40			18			32				17	45	
64	16 24 27.4	-24 32 36										16	46	
65	16 24 28.8	-24 21 4			17			33				17	47	
66	16 24 35.5	-24 23 55										46	48	
67	16 24 36.4	-24 24 1										46	50	
68	16 24 36.4	-24 30 18								C20		47	49	
69	16 24 37.6	-24 36 35										45	51	
70	16 24 38.8	-24 15 24	9				29	34		29	54	49	52	
71	16 24 48.3	-24 19 2			14		31	36				53		
72	16 24 50.0	-24 25 5										52	54	
73	16 24 50.3	-24 34 10								31			55	binary
74	16 24 50.3	-24 34 10								31			55	
75	16 24 53.9	-24 19 40	10				33				57	56?		
76	16 25 14.6	-24 30 21									60	58		
77	16 25 31.1	-24 16 10	20				38			33	61	60?		
78	16 25 51.9	-24 41 10									63			

TABLE A1 (CON'T)

[1]Notes to Table A1. Columns (2) and (3) give the Epoch 1950 positions determined from optical or near-infrared telescopes and have typical uncertainties of a few arcseconds. Columns (4) -(14) give source numbers from Struve and Rudkjobing (SR, 1949), Grasdalen, Strom, and Strom (GSS, 1973), Vrba *et al*. (VSSG, 1975), Vrba, Strom, and Strom (VSS, 1976), Chini (Cl, 1981), Elias (EL, 1978), Wilking and Lada (WL, 1983), Montmerle et al. (ROX, 1983), Wilking, Schwartz, and Blackwell ($H\alpha$, 1987), Young, Lada, and Wilking (YLW, 1986) and this study for IRAS sources, and this study for and 2 μm sources (IRS, Table 2). Column 15 gives other names including "Source" designations by GSS and VS, and denotes binary star systems found during a lunar occultation (Simon *et al*. 1987).

TABLE A2

A Cross Reference List of Field Stars

	R.A. (1950)	Dec(1950)	GSS	VSSC	VSS	C1	EL	IRAS	IRS	other
1	$16^h 22^m 34.^s0$	−24°27'13"	15			6	11		1	S16
2	16 23 4.0	−24 36 9					15	27		
3	16 24 45.2	−24 16 43		13		30	35			
4	16 25 2.1	−24 19 54		16	34	34	37	56?	58	
5	16 25 7.8	−24 16 44		15		36	38			

TABLE A3

A Cross Reference List of Unidentified Sources

	R.A. (1950)	Dec(1950)	SR	GSS	VSSG	VSS	CI	EL	WL	ROX	IRAS/YLW	IRS
	h m s											
1	16 22 36.7	-24° 6'56"						12				
2	16 22 38.0	-24 19 46										3
3	16 22 38.7	-24 10 17										4
4	16 22 39.3	-24 19 29										5
5	16 22 39.5	-24 9 58										6
6	16 22 54.5	-24 23 28										11
7	16 22 56.8	-24 11 1			19		9					
8	16 23 6.8	-24 8 1			20		11					
9	16 23 36.7	-24 16 22			4							
10	16 23 39.1	-24 24 6										16
11	16 23 40.3	-24 26 41							8			
12	16 23 41.2	-24 17 44										18
13	16 23 44.7	-24 16 24			28							
14	16 23 47.4	-24 31 34							18			
15	16 23 49.7	-24 14 7									1	20
16	16 23 50.7	-24 8 4			10							
17	16 23 52.3	-24 15 44		40	6					C12		21
18	16 23 53.9	-24 13 45		41	7						1	22
19	16 23 56.9	-24 14 47									1	26
20	16 24 0.1	-24 14 54			8							28
21	16 24 0.7	-24 12 14			9		22					
22	16 24 2.8	-24 13 24			21		23					
23	16 24 4.1	-24 19 37									10	30
24	16 24 8.3	-24 38 50	25			30						
25	16 24 10.1	-24 16 59										32
26	16 24 11.8	-24 36 49										32b
27	16 24 12.8	-24 11 34			24		26					
28	16 24 12.8	-24 20 4										33
29	16 24 13.8	-24 24 12										35
30	16 24 13.9	-24 18 33									10	36
31	16 24 16.5	-24 22 9			26				5		12	38
32	16 24 41.6	-24 36 28										53
33	16 24 50.8	-24 41 16									54	56
34	16 24 58.3	-24 15 20										57
35	16 25 8.9	-24 9 23	15			35	37					
36	16 25 43.9	-24 41 21				38						
37	16 25 57.2	-24 42 35				39						
38	16 26 11.2	-24 17 22				42						
39	16 26 43.6	-24 13 20				41						

References

Adams, F. C., and Shu, F. H. 1986, *Ap. J.*, **308**, 836.

Adams, F. C., Lada, C. J., and Shu F. H. 1987, *Ap. J.*, **312**, 788.

Adams, F. C., Lada, C. J., and Shu, F. H. 1988, *Ap. J.*, **326**, 865.

Beall, J. H. 1987, *Ap. J.*, **316**, 227.

Chini, R. 1981, *Astr. Ap.*, **99**, 346.

Cohen, M. and Kuhi, L. V. 1979, *Ap. J. Suppl.*, **41**, 743.

Cudlip, W., Emerson, J.P., Furniss, I., Glencross, W. M., Jennings, R. E., King, K. J., Lightfoot, J. F., and Towlson, W.A. 1985, *M.N.R.A.S.*, **211**, 563.

Dickman, R.L. 1978, *Ap. J. Suppl.*, **37**, 407.

Disney, M. J. and Sparks, W. B. 1982, *Observatory*, **102**, 234.

Duerr, R., Imhoff, C. L. and Lada, C. J. 1982, *Ap.J.*, **261**, 135.

Dolidze, M. V., and Arakelyan, M. A. 1959, *Soviet Astr.-AJ*, **3**, 434.

Elias, J. H. 1978, *Ap. J.*, **224**, 453.

Emerson, J. P. 1988, in *Formation and Evolution of Low Mass Stars*, ed. A. Dupree and M.T.V.T. Lago (Boston: D. Reidel), in press.

Fazio, G. G., Wright, E. L., Zielik, M., III, and Low, F. J. 1976, *Ap. J. (Letters)*, **206**, L165.

Frerking, M. A., Langer, W. D., and Wilson, R. W. 1982, *Ap. J*, **262**, 590.

Garrison, R. F. 1967, *Ap. J.*, **147**, 1003.

Grasdalen. G. L., Strom, K. M., and Strom, S.E. 1973, *Ap. J. (Letters)*, **184**, L53.

Harris, D. H., Woolf, N, J., and Rieke, G. H. 1978, *Ap. J.*, **226**, 829.

Harvey, P. M., Wilking, B. A., and Joy, M. 1984, *Ap. J.*, **278**, 156.

Herbig, G. H., Vrba, F. J., and Rydgren, A.E. 1986, *A.J.*, **91**, 575.

Iben, I., Jr. 1965, *Ap. J.*, **141**, 993.

IRAS Point Source Catalog 1985, *Joint IRAS Science Working Group*, (Washington D. C.: U.S. Government Printing Office).

Jones, B. F. and Herbig, G. H. 1979, *A. J.*, **84**, 1872.

Kenyon, S. J., and Hartmann, L. 1987, *Ap. J.*, **323**, 714.

Lada, C. J. 1987, in *Star Forming Regions*, ed. M. Peimbert and J. Jugaku (Boston: D. Reidel), p.1.

Lada, C. J. 1988, in *Formation and Evolution of Low Mass Stars*, ed. A. Dupree and M.T.V.T. Lago (Boston: D. Reidel), in press.

Lada, C. J., Margulis, M., and Dearborn, D. 1984, *Ap. J.*, **285**, 141.

Lada, C. J., and Wilking, B. A. 1984, *Ap. J.*, **287**, 610.

Loren, R. B. 1988, *in preparation*, .

Miller, G. E. and Scalo, J. M. 1979, *Ap. J. Suppl.*, **41**, 513.

Montmerle, T., Koch-Miramonde, L., Falgarone, E., and Grindlay, J. E. 1983, *Ap. J.*, **269**, 182.

Myers, P. M., Fuller, G. A., Mathieu, R. D., Beichmann, C. A., Benson, P. J., Schild, R. E., and Emerson, J. P 1987, *Ap. J.*, **319**, 340.

Rieke, G. H. and Lebofsky, M. J. 1985, *Ap. J.*, **288**, 618.

Rucinski, S.M. 1985, *A. J.*, **90**, 2321.

Rydgren, A.E. 1980, *A.J.*, **85**, 438.

Rydgren, A. E., Schmelz, J. T., Zak, D. S., and Vrba, F. J. 1984, *Publ. U.S. Naval. Obs.* (15: Part 1).

Rydgren, A. E., Strom, S. E., and Strom, K.M. 1976, *Ap. J. Suppl.*, **30**, 307.

Salpeter, E. E. 1955, *Ap. J.*, **121**, 161.

Scalo, J. M. 1986, *Fundamentals of Cosmic Physics*, **11**, 1.

Shu, F. H., Adams, F. C., and Lizano, S. 1987, *Ann. Rev. Astr. Ap.*, **25**, 23.

Simon, M., Howell, R. R., Longmore, A. J., Wilking, B. A., Peterson, D. M., and Chen, W. P. 1987, *Ap. J.*, **320**, 344.

Stahler, S. W. 1983, *Ap. J.*, **274**, 822.

Stahler, S. W., Shu, F. H., and Taam, R. E. 1980, *Ap. J.*, **241**, 637.

Strom, K. M., Strom, S. E., Kenyon, S. J., and Hartmann, L. 1988, *A. J.*, **95**, 534.

Struve, O. and Rudkjobing, M. 1949, *Ap. J.*, **109**, 92.

Vrba, F. J., Strom, S. E., and Strom, K. M. 1976, *A. J.*, **81**, 958.

Vrba, F. J., Strom, K. M., Strom, S. E., and Grasdalen, G. L. 1975, *Ap. J.*, **197**, 77.

Walter, F. M. 1986, *Ap. J.*, **306**, 573.

Walter, F. M., Brown, A., Mathieu, R. D., Myers, P. C., and Vrba, F. J. 1988, *A. J.*, **96**, 297.

Wilking, B. A. and Lada, C. J. 1983, *Ap. J.*, **274**, 698.

Wilking, B. A., Schwartz, R. D., and Blackwell, J. H. 1987, *A. J.*, **94**, 106.

Young, E. T., and Greene, T. 1988, *Ap. J.*, in press.

Young, E. T., Lada, C. J., and Wilking, B. A. 1986, *Ap. J. (Letters)*, **304**, L45.

Figure Captions

Figure 1 - The distribution of IRAS 12 μm emission relative to visual extinction and molecular gas in the central regions of the ρ Ophiuchi dark cloud. Figure 1a is an overlay of the 12 μm point and small extended source positions with the red photograph from the Palomar Sky Survey. Large crosses mark the positions of sources with 12 μm flux densities greater than 0.25 Jy and small crosses less than this value. The boundaries of the molecular gas are shown by a solid contour which encompasses a 4.3 pc^2 area where $^{13}CO(1-0)$ emission line strengths of $T_R^* \geqslant 6$ K (Loren 1988). Figure 1b shows the unfiltered intensity map of the 12 μm emission over the same area as above. The contour levels for the 12 μm emission are 1.78E5* (-15, -10, -5, 3, 6, 10, 20, 40, 80, 160, 320, 640, 1280, 2560) in units of Jy/sr. The shaded area delineates the molecular cloud.

Figure 2 - In-scan slices of IRAS 34 at 12 and 25 μm.

Figure 3 - Spectral energy distributions for 32 association members of the ρ Oph cluster displaying IRAS emission, grouped according to their spectral index as defined by $a = d\log(\lambda F_\lambda)/d\log\lambda$. Source names accompanying each spectrum are given for both the near-infrared and IRAS designations (see footnotes to Tables 1 and 2 for references to source names). The power of ten used to scale the spectral energy distribution is given in parantheses below the source name. In addition to the references in Table 1, photometric data was adopted from Chini (1981), Harris, Woolf, and Rieke (1978), Rydgren, Strom, and Strom (1976), and Rydgren (1980). Figure 3a shows energy distributions for $3 > a > 1$, Figure 3b for $1 > a > 0$, Figures 3c and 3d for $0 > a > -1.5$, and Figure 3e for double-peaked sources. For comparison, blackbody energy distributions are presented in Figure 3d and 3e.

Figure 4 - The distribution of spectral indices for 48 association members and 5 field or unidentified objects toward the ρ Oph cloud.

Figure 5 - The luminosity function for 74 members of the ρ Oph embedded cluster. For comparison, the luminosity function derived from the IMF is shown, normalized to the number of objects with well-determined luminosities in the $-0.25 < \log L''(\mathrm{obs}) < 0.75$ range. The sources in each luminosity bin are broken down by the morphology of their SED. Luminosity estimates which are upper limits are also shown but not included in the normalization of the ILF.

Figure A1 - A classification scheme to differentiate between association members and background field stars found toward the ρ Oph cloud.

Figure A2 - Spectral energy distributions for background field stars found by Elias (1978) and this study toward the ρ Oph cloud. Most of the energy distributions are unreddened and resemble that of a single temperature blackbody shown at the bottom of the plot.

Figure A3 - The distribution of association members in the ρ Oph cloud superposed on the red photograph of the Palomar Sky Survey. Unlike Fig. 1a, the molecular cloud outlined in the figure is not uniformly sampled by high sensitivity infrared surveys at 2.2 μm.

Authors' Postal Addresses

Charles J. Lada and Erick T. Young: Steward Observatory, University of Arizona, Tucson, AZ 85721.

Bruce A. Wilking: Department of Physics, University of Missouri-St. Louis, St. Louis, MO 63121

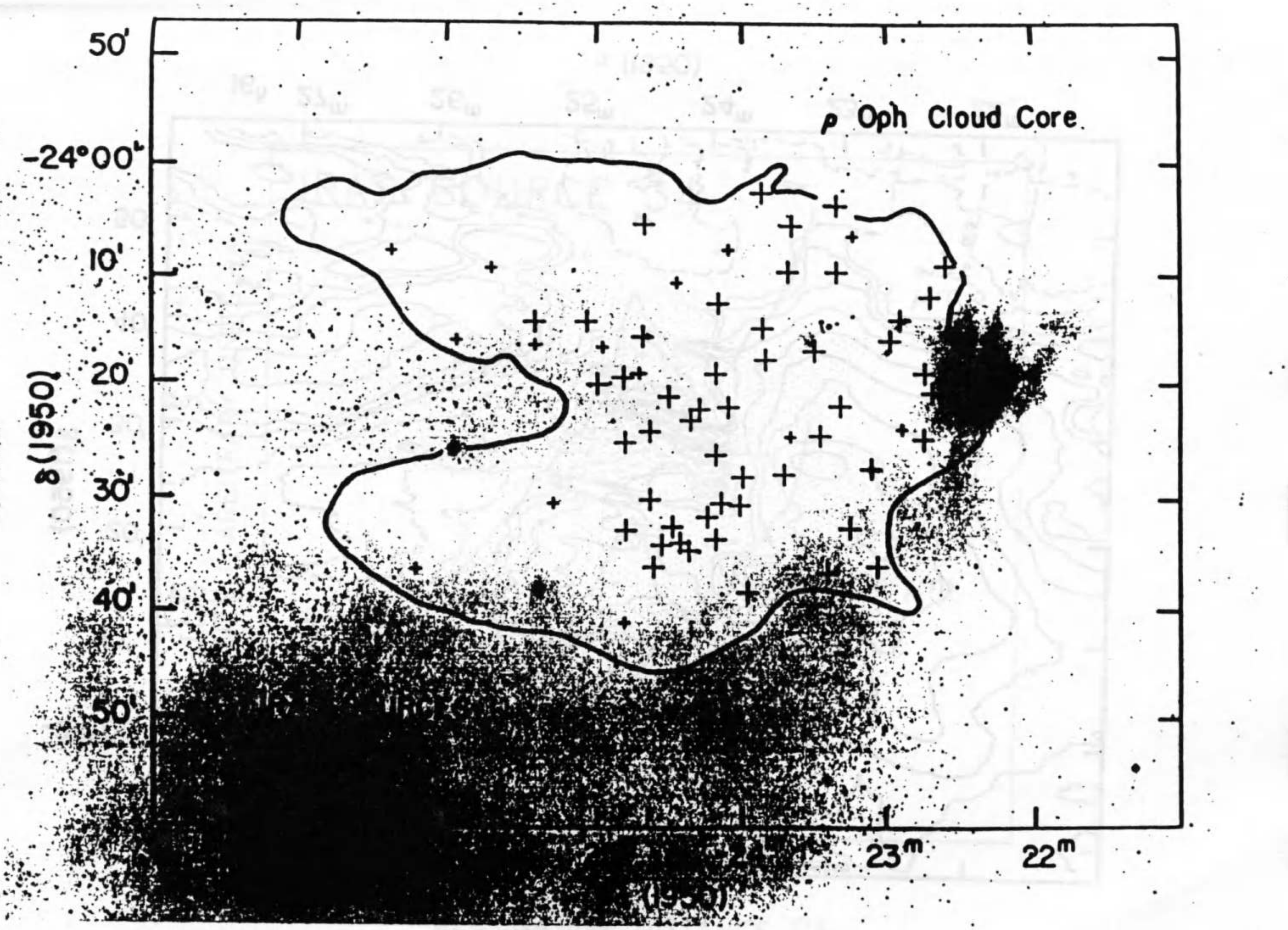

Figure 1a

Figure 1b

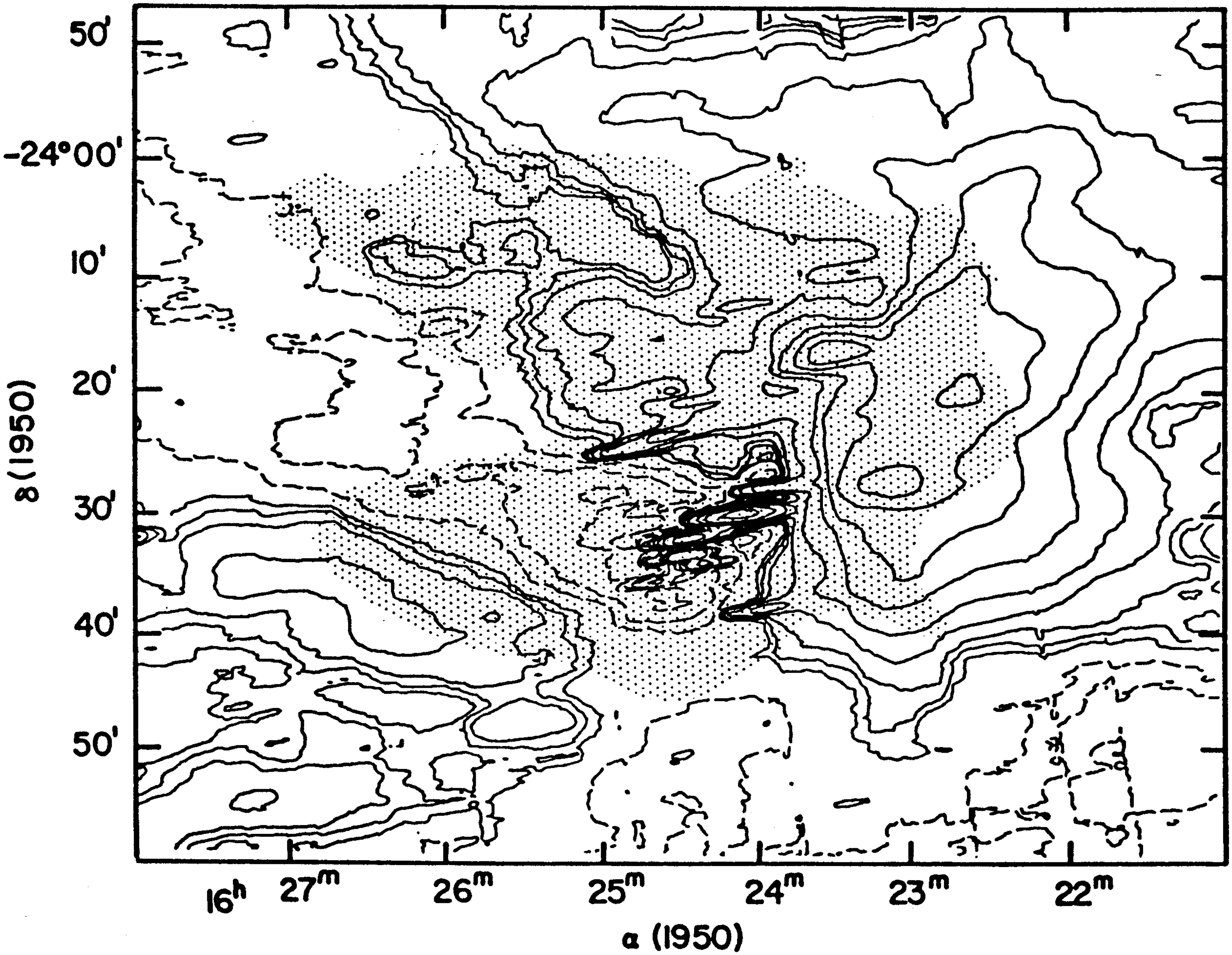

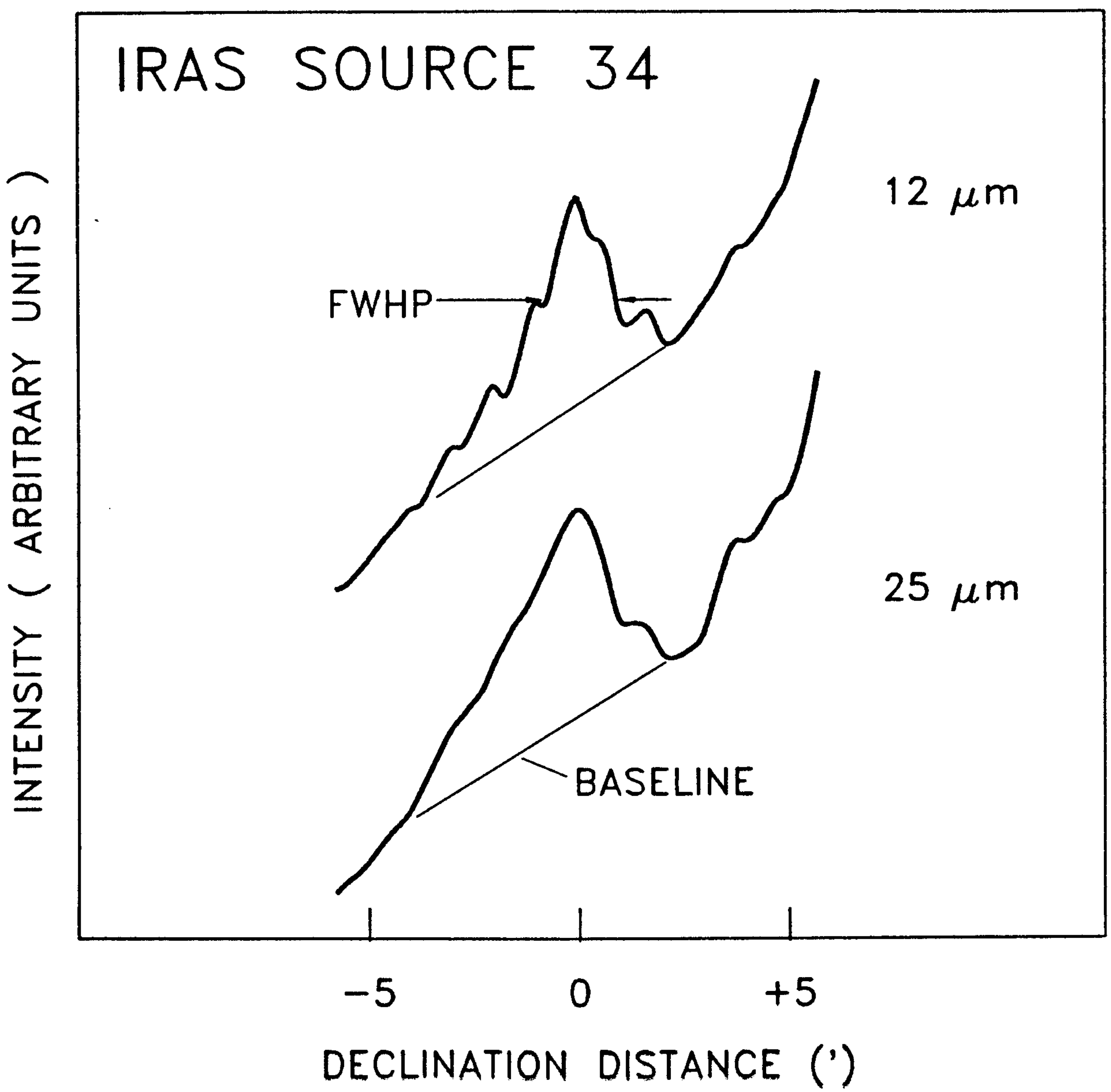
IRAS SOURCE 34
12 μm
25 μm
FWHP
BASELINE
INTENSITY (ARBITRARY UNITS)
−5
0
+5
DECLINATION DISTANCE (')

Figure 2

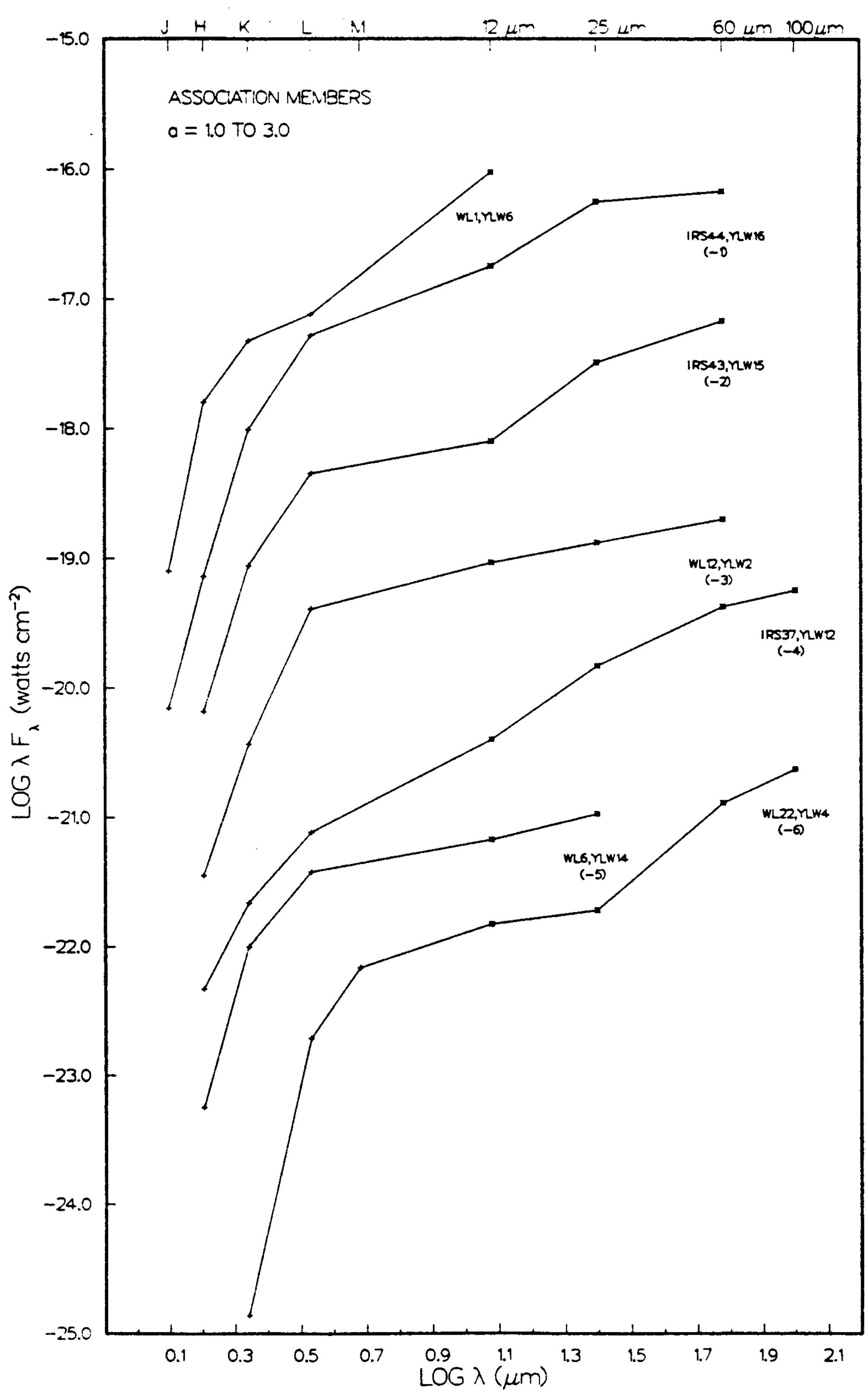

J
H
K
L
M
12 μm
25 μm
60 μm
100μm
ASSOCIATION MEMBERS
a = 1.0 TO 3.0
WL1,YLW6
IRS44,YLW16
(−1)
IRS43,YLW15
(−2)
WL12,YLW2
(−3)
IRS37,YLW12
(−4)
WL6,YLW14
(−5)
WL22,YLW4
(−6)
−15.0
−16.0
−17.0
−18.0
−19.0
−20.0
−21.0
−22.0
−23.0
−24.0
−25.0
LOG λ F_λ (watts cm^−2)
0.1
0.3
0.5
0.7
0.9
1.1
1.3
1.5
1.7
1.9
2.1
LOG λ (μm)

Figure 3a

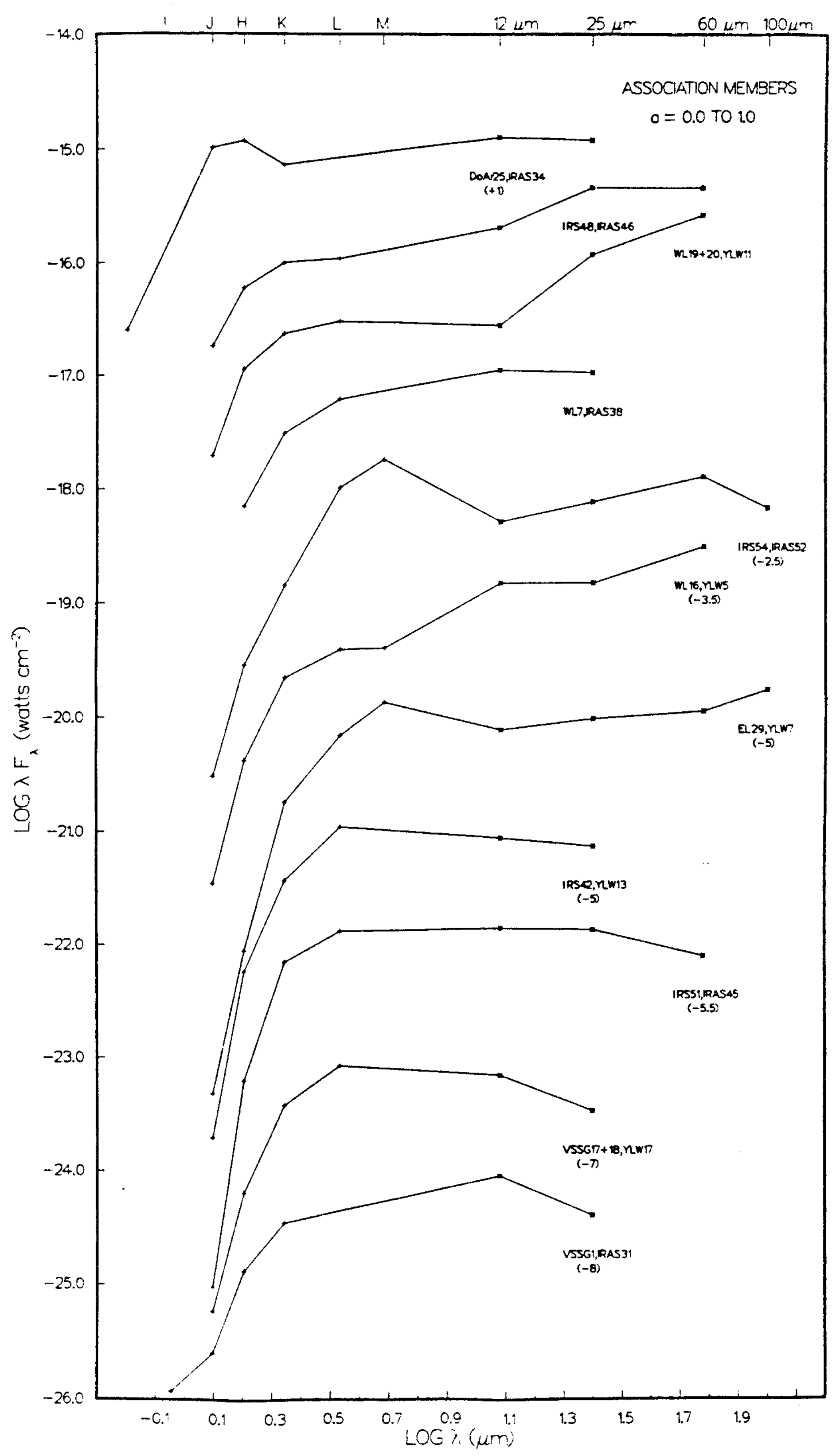

ASSOCIATION MEMBERS
a = 0.0 TO 1.0
DoAr25,IRAS34 (+1)
IRS48,IRAS46
WL19+20,YLW11
WL7,IRAS38
IRS54,IRAS52 (-2.5)
WL16,YLW5 (-3.5)
EL29,YLW7 (-5)
IRS42,YLW13 (-5)
IRS51,IRAS45 (-5.5)
VSSG17+18,YLW17 (-7)
VSSG1,IRAS31 (-8)
I J H K L M 12 μm 25 μm 60 μm 100μm
LOG λ F$_λ$ (watts cm^{-2})
LOG λ (μm)

Figure 3b

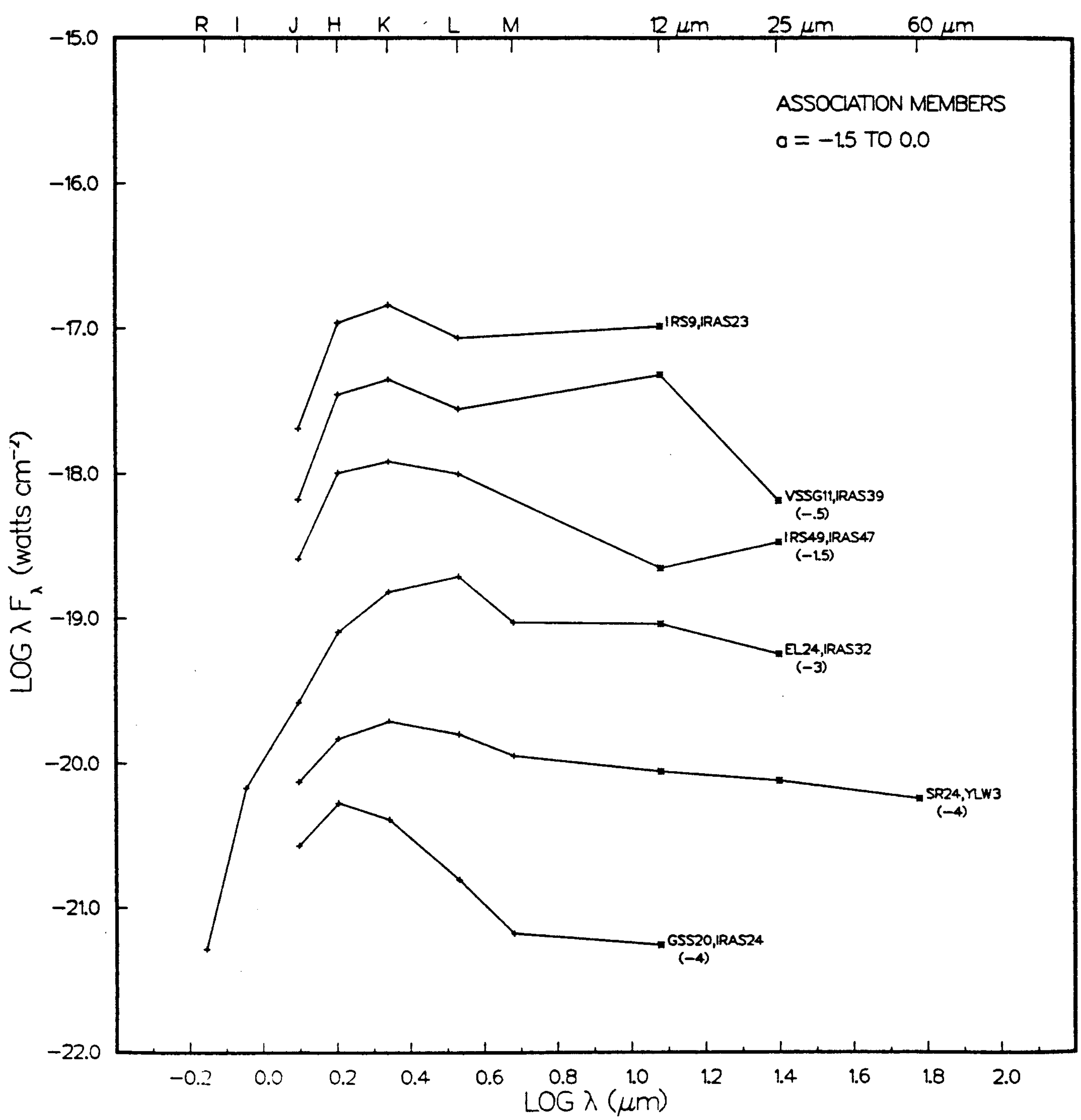
R
I
J
H
K
L
M
12 μm
25 μm
60 μm
ASSOCIATION MEMBERS
α = −1.5 TO 0.0
IRS9,IRAS23
VSSG11,IRAS39
(−.5)
IRS49,IRAS47
(−1.5)
EL24,IRAS32
(−3)
SR24,YLW3
(−4)
GSS20,IRAS24
(−4)
LOG λ Fλ (watts cm−2)
−15.0
−16.0
−17.0
−18.0
−19.0
−20.0
−21.0
−22.0
−0.2
0.0
0.2
0.4
0.6
0.8
1.0
1.2
1.4
1.6
1.8
2.0
LOG λ (μm)

Figure 3c

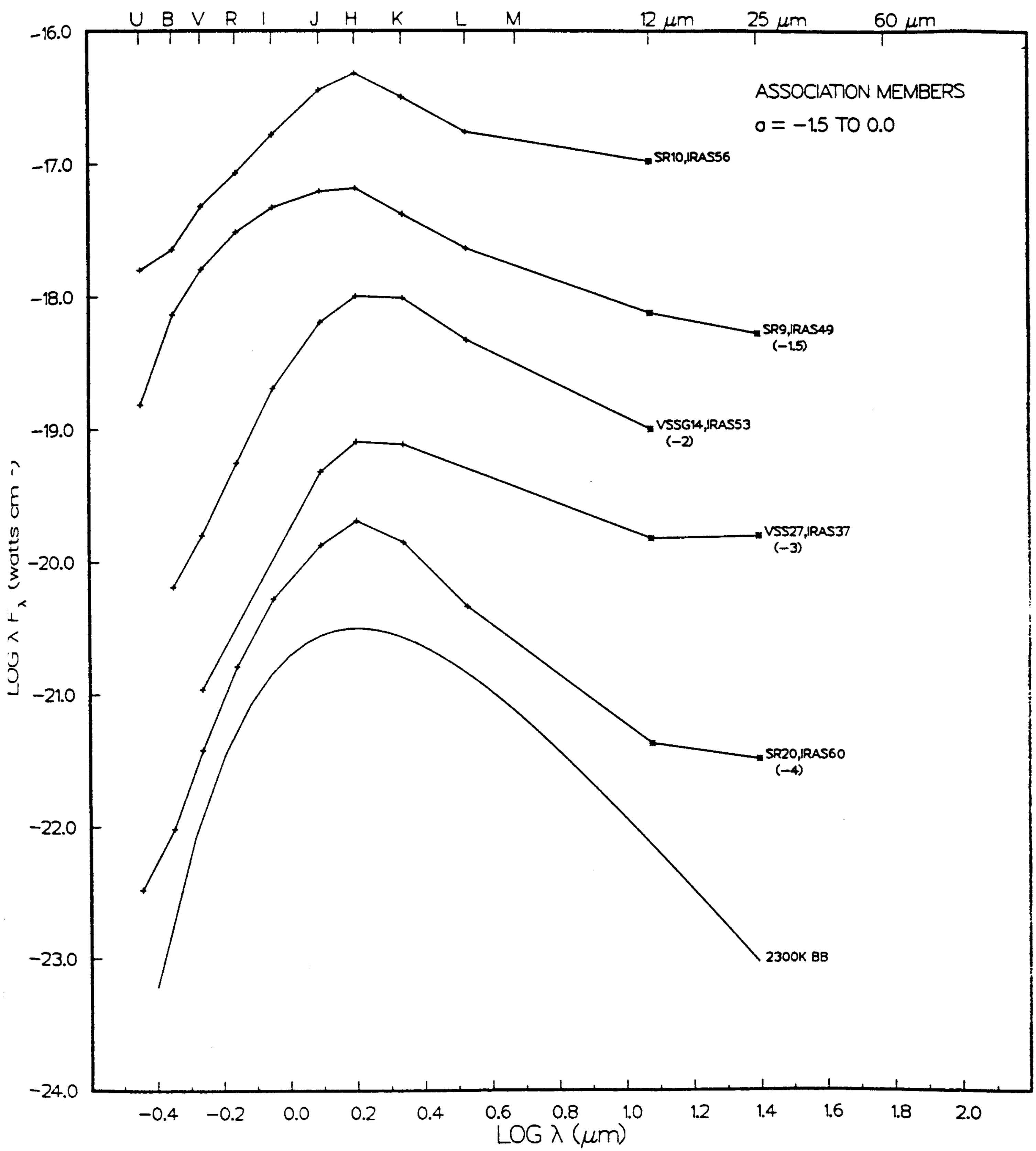
U B V R I J H K L M 12 μm 25 μm 60 μm
ASSOCIATION MEMBERS
a = −1.5 TO 0.0
SR10,IRAS56
SR9,IRAS49
(−1.5)
VSSG14,IRAS53
(−2)
VSS27,IRAS37
(−3)
SR20,IRAS60
(−4)
2300K BB
LOG λ F λ (watts cm ⁻)
−16.0
−17.0
−18.0
−19.0
−20.0
−21.0
−22.0
−23.0
−24.0
−0.4 −0.2 0.0 0.2 0.4 0.6 0.8 1.0 1.2 1.4 1.6 1.8 2.0
LOG λ (μm)

Figure 3d

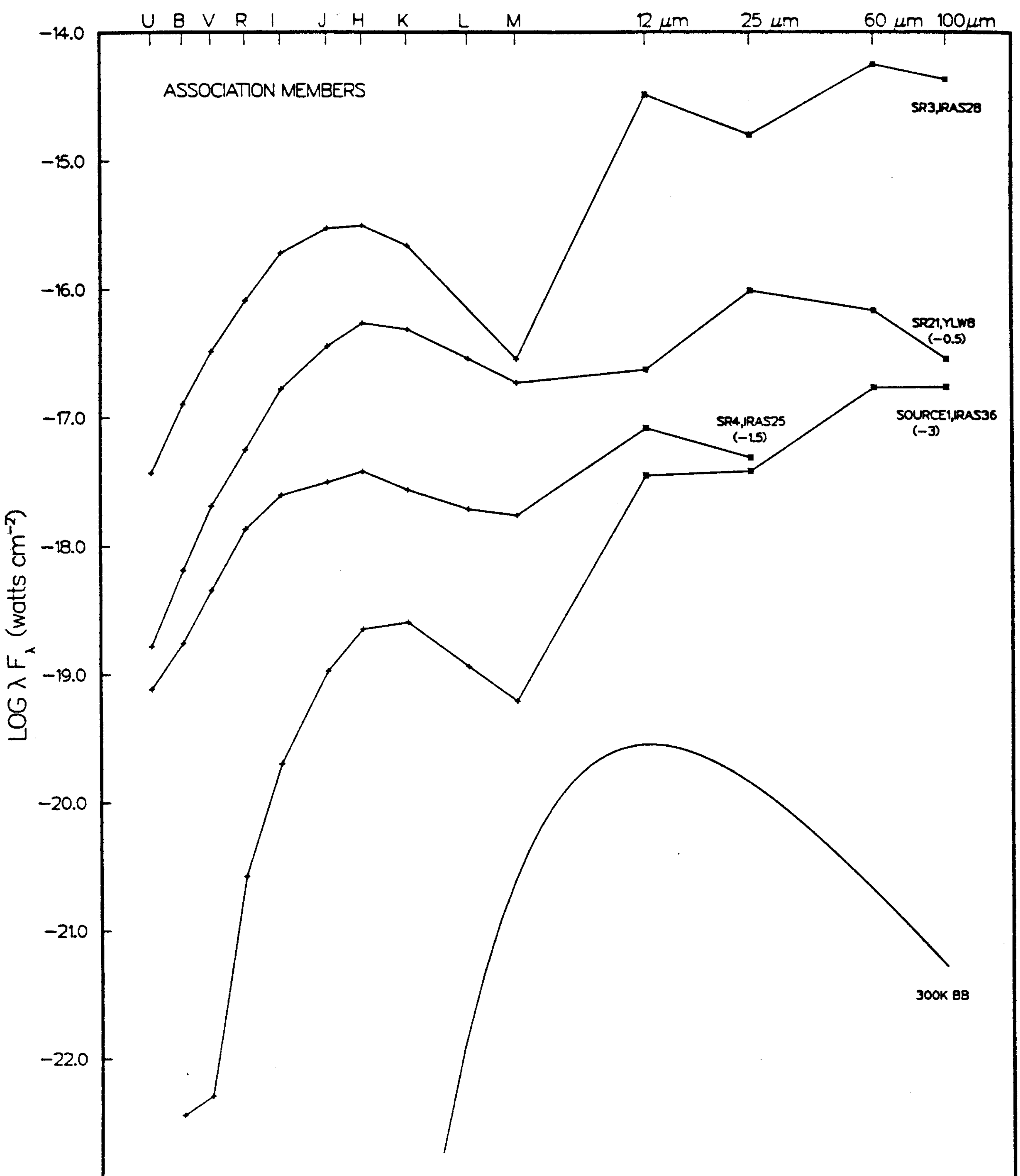
U B V R I J H K L M 12 μm 25 μm 60 μm 100μm
ASSOCIATION MEMBERS
SR3,IRAS28
SR21,YLW8
(−0.5)
SR4,IRAS25
(−1.5)
SOURCE1,IRAS36
(−3)
300K BB
LOG λ F$_\lambda$ (watts cm^{-2})
−14.0
−15.0
−16.0
−17.0
−18.0
−19.0
−20.0
−21.0
−22.0
−23.0
−0.4 −0.2 0.0 0.2 0.4 0.6 0.8 1.0 1.2 1.4 1.6 1.8 2.0
LOG λ (μm)

Figure 3e

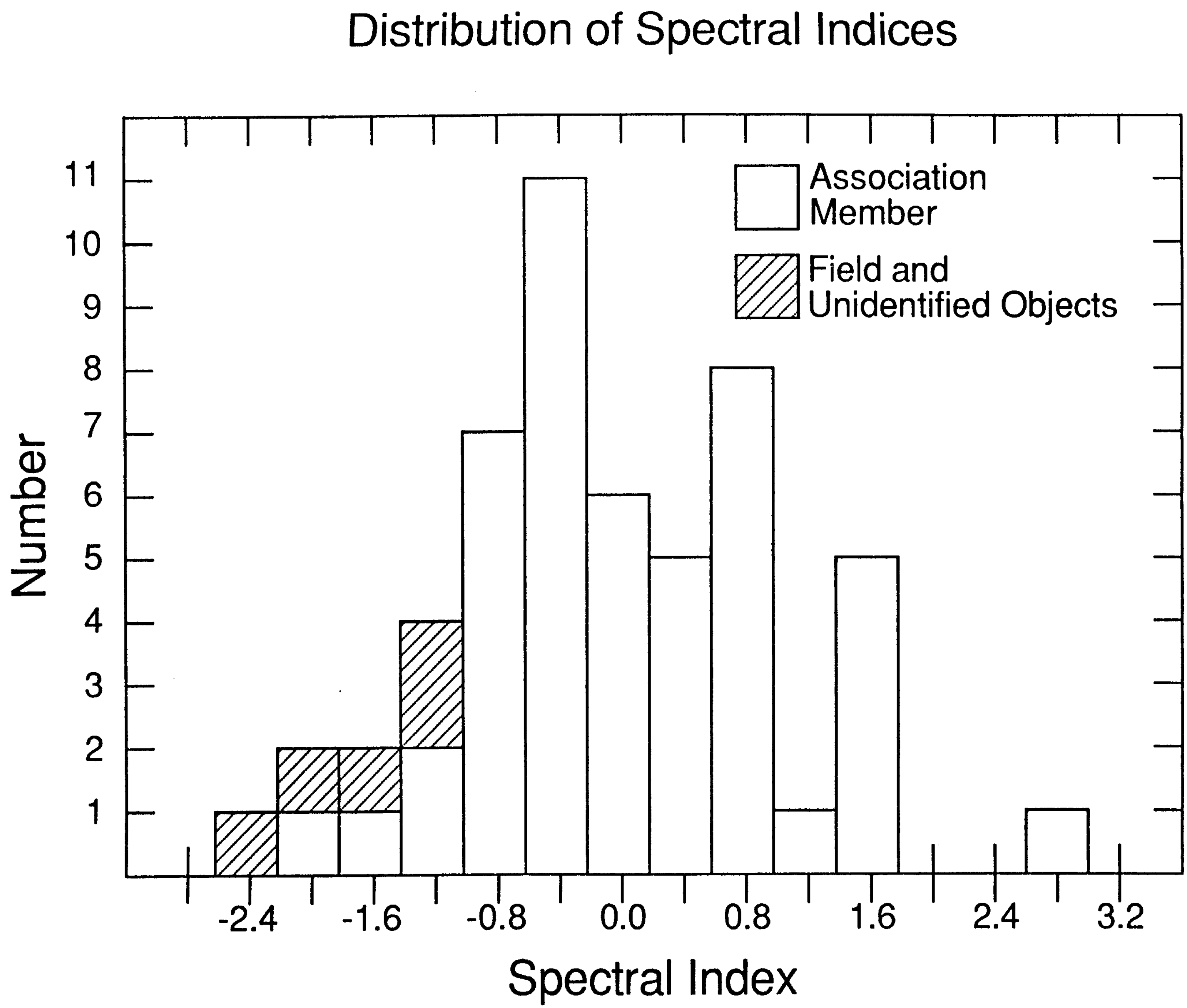
Distribution of Spectral Indices
Association Member
Field and Unidentified Objects
Number
Spectral Index
11
10
9
8
7
6
5
4
3
2
1
-2.4
-1.6
-0.8
0.0
0.8
1.6
2.4
3.2

Figure 4

Figure 5

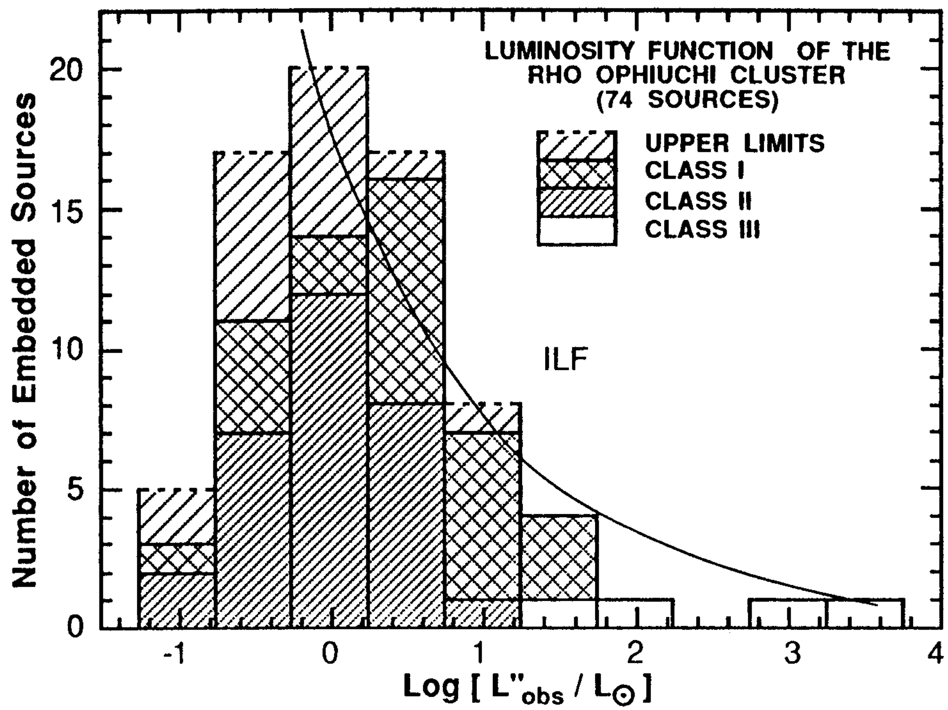
LUMINOSITY FUNCTION OF THE
RHO OPHIUCHI CLUSTER
(74 SOURCES)
UPPER LIMITS
CLASS I
CLASS II
CLASS III
ILF
Number of Embedded Sources
0
5
10
15
20
-1
0
1
2
3
4
Log [L"obs / L☉]

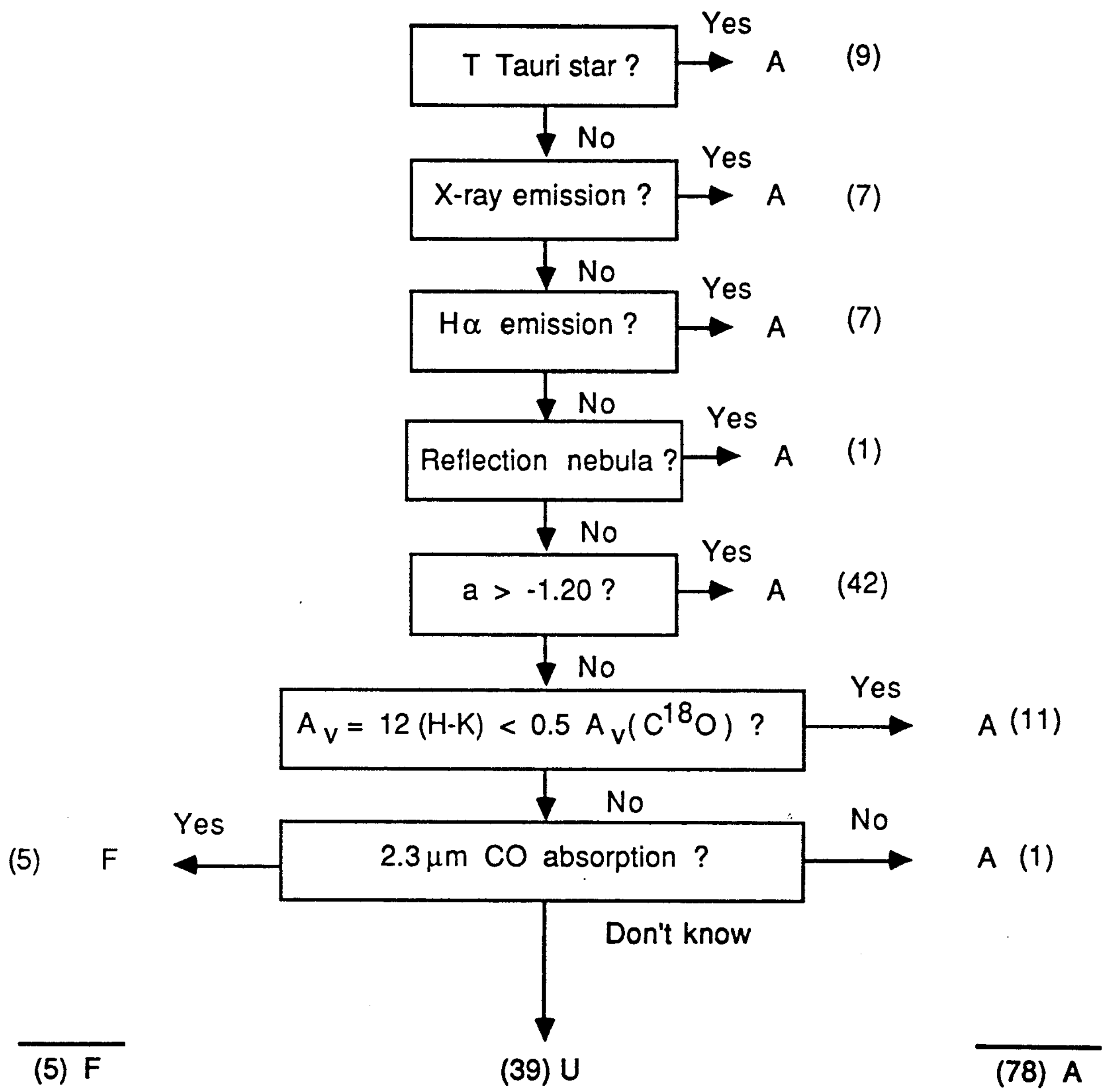
T Tauri star ?
Yes
A
(9)
No
X-ray emission ?
Yes
A
(7)
No
Hα emission ?
Yes
A
(7)
No
Reflection nebula ?
Yes
A
(1)
No
a > -1.20 ?
Yes
A
(42)
No
A V = 12 (H-K) < 0.5 A V(C18O) ?
Yes
A (11)
No
2.3 μm CO absorption ?
Yes
(5) F
No
A (1)
Don't know
(5) F
(39) U
(78) A

Figure A1

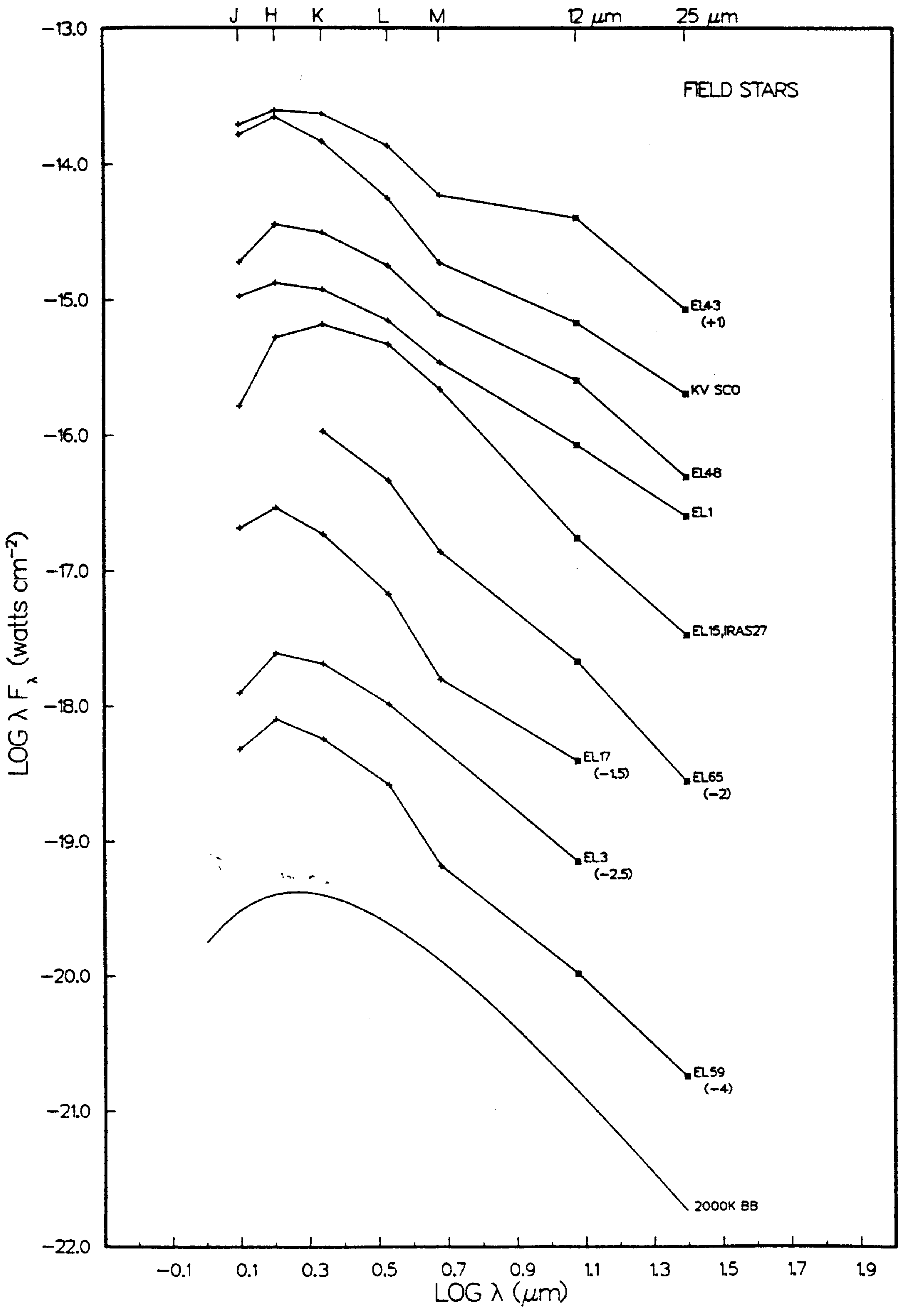
J
H
K
L
M
12 μm
25 μm
FIELD STARS
EL43
(+0)
KV SCO
EL48
EL1
EL15,IRAS27
EL17
(−1.5)
EL65
(−2)
EL3
(−2.5)
EL59
(−4)
2000K BB
−13.0
−14.0
−15.0
−16.0
−17.0
−18.0
−19.0
−20.0
−21.0
−22.0
LOG λ F$_\lambda$ (watts cm^{-2})
−0.1
0.1
0.3
0.5
0.7
0.9
1.1
1.3
1.5
1.7
1.9
LOG λ (μm)

Figure A2

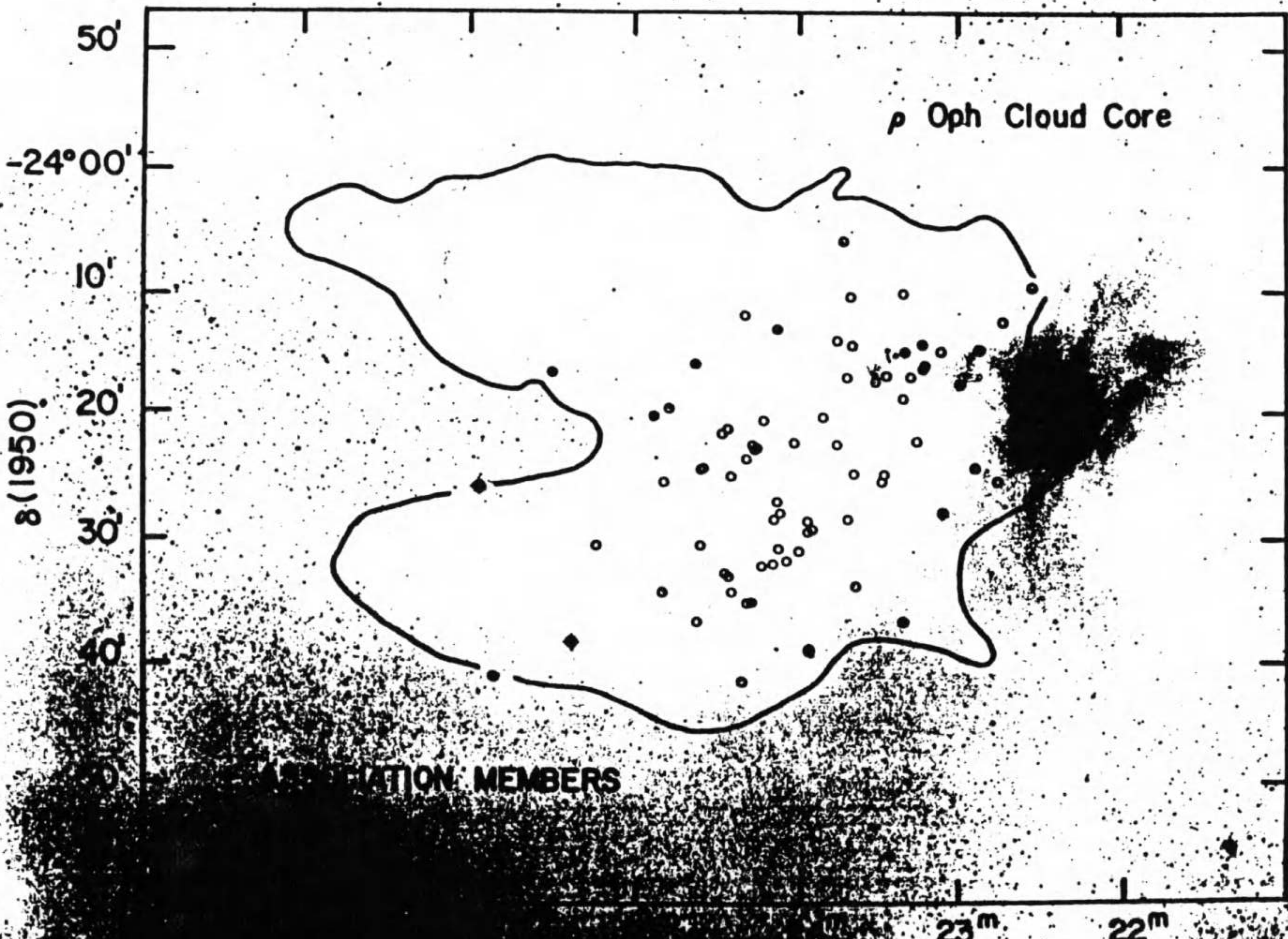

Figure A3